3-2003

A Study of Control Laws for Microsatellite Rendezvous with a Non-Cooperative Target

Troy A. Tschirhart

A STUDY OF CONTROL LAWS FOR MICROSATELLITE RENDEZVOUS WITH A NONCOOPERATIVE TARGET

THESIS

Troy A. Tschirhart, Major, USAF

AFIT/GAI/ENY/03-3

DEPARTMENT OF THE AIR FORCE

AIR UNIVERSITY

AIR FORCE INSTITUTE OF TECHNOLOGY

Wright-Patterson Air Force Base, Ohio

The views expressed in this thesis are those of the author and do not reflect the official policy or position of the United States Air Force, Department of Defense, or the United States Government.

AFIT/GAI/ENY/03-3

A STUDY OF CONTROL LAWS FOR MICROSATELLITE RENDEZVOUS WITH A NONCOOPERATIVE TARGET

THESIS

Presented to the Faculty

Department of Aeronautics and Astronautics

Graduate School of Engineering and Management

Air Force Institute of Technology

Air University

Air Education and Training Command

In Partial Fulfillment of the Requirements for the

Degree of Master of Science in Astronautical Engineering

Troy A. Tschirhart

Major, USAF

March 2003

AFIT/GAI/ENY/03-3

A STUDY OF CONTROL LAWS FOR MICROSATELLITE RENDEZVOUS WITH A NONCOOPERATIVE TARGET

Troy A. Tschirhart, BS
Major, USAF

Approved:

//SIGNED//	13 Mar 03
Dr Steven Tragesser Thesis Advisor	Date
//SIGNED//	13 Mar 03
Maj Richard Cobb Committee Member	Date
//SIGNED//	13 Mar 03
Dr William Wiesel Committee Member	Date

Acknowledgements

I would like to thank my advisor, Dr Steven Tragesser, for all of his guidance and patience throughout the challenging thesis process.

I would also like to thank my fellow Vigilant Scholars, Brian, Brian, JD and Jenna, along with all of the other students in section ENY-03M, who helped me to keep it all in perspective.

Table of Contents

Page

List of Figures

Page

Page

List of Tables

Page

Page

Abstract

The feasibility of using a microsatellite to accomplish an orbital rendezvous with a noncooperative target is being evaluated. This study focused on the control laws necessary for achieving such a rendezvous. The relative motions of the microsatellite and the target satellite were described using Hill's equations and two different controller methodologies were investigated. An impulsive thrust controller based on the Clohessey-Wiltshire solution was found to use little fuel, but was not very robust. A continuous thrust controller using a Linear Quadratic Regulator was found to be more robust, but used much more fuel. As a final solution, a hybrid controller was evaluated which uses the low thrust Clohessey-Wiltshire approach to cover most of the necessary distance, and then switches to the Linear Quadratic Regulator method for the final rendezvous solution. Results show that this approach achieves rendezvous with a reasonable amount of control input.

A STUDY OF CONTROL LAWS FOR MICROSATELLITE RENDEZVOUS WITH A NONCOOPERATIVE TARGET

I. Introduction

Background

The United States derives great benefit from space-based assets, and U.S. dependence on space-based capabilities will only continue to increase. Other countries who recognize the advantage conferred on the U.S. by its space prowess may wish to develop the means to neutralize it.

One potential method would be to use a parasitic satellite. A parasitic satellite would rendezvous with, and potentially attach to a target satellite, where it would await a command from the ground to either disrupt satellite operations or destroy the satellite.

The Chinese claim to be developing microsatellites to perform this role. (7) The concept of operations would likely begin with a ground-based orbit determination of the target satellite. Then, a microsatellite would either be launched or released from a mother ship that is already on orbit. Finally, the microsatellite would autonomously achieve rendezvous and attach to the target.

Microsatellites have a mass of 100 kg or less, and are less expensive to build and launch than larger satellites. However, an inherent limitation in such a small vehicle is

fuel capacity. Therefore, the control laws used to achieve rendezvous should minimize fuel usage to the maximum extent possible.

Problem Description

In an effort to assess the threat posed, this study focuses on the control laws necessary for a microsatellite to achieve orbital rendezvous with a non-cooperative target. Other aspects of microsatellite capabilities are being studied by other researchers. Once all of the various investigations have been completed, it is expected that the compilation of results will indicate the overall feasibility of the proposed system.

For this project, it is assumed that the microsatellite will be placed into an orbit similar to that of the target satellite, approximately 1000 km behind it in the same orbital plane. The microsatellite then performs rendezvous maneuvers to approach the target.

For this project, it is assumed that the microsatellite has perfect knowledge of the target's position and velocity at all times. In reality, the microsatellite would likely begin with an orbit solution derived from off-board sensors. As the microsatellite approached the target, onboard sensors would detect the target satellite and an updated orbit solution would be calculated. This would allow the microsatellite to complete the rendezvous without any feedback from the target satellite. Future work on this topic should include accounting for the uncertainties that would exist in reality.

This study begins with satellite dynamics; then, the considered control methodologies are discussed. Finally, the controllers are employed and the results evaluated.

II. Dynamics

Coordinate Frames

Three different coordinate frames are used throughout this project. The first is the Earth Centered Inertial (ECI) frame, which is depicted in Figure 1. The ECI frame is inertially fixed in space and has its origin at the center of the Earth. The first axis in the ECI frame points toward the vernal equinox, the second axis is normal to the first in the equatorial plane, in a direction that completes the frame with the third axis pointing out of the North Pole.

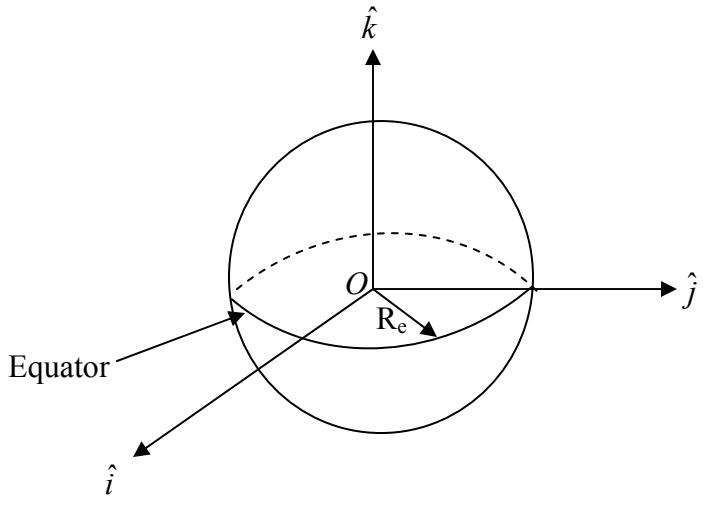

Figure 1 Earth Centered Inertial (ECI) Coordinate Frame

A second coordinate frame is the Perifocal frame (PQW). The PQW frame also has its origin at the center of the Earth, but the first two axes are in the orbital plane of interest. The first axis points toward perigee and the second axis is perpendicular to the first such that the third axis points in the direction of the cross product of the satellite's position and velocity vectors. This frame is shown in Figure 2.

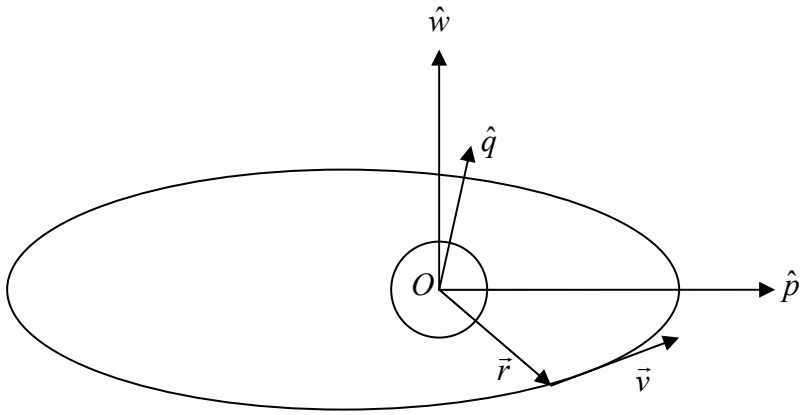

Figure 2 Perifocal (PQW) Coordinate Frame

The third coordinate frame used in this project is Hill's (RTZ) coordinate frame. Hill's coordinate frame is also in the plane of the orbit of interest, but it includes a reference orbit which must be circular. A reference origin moves about the circular orbit with mean motion, n. The first axis points in the radial direction, the second axis points in the direction of the instantaneous velocity, and the third axis points in the out of plane direction corresponding to the cross product between the first two axes. Hill's Coordinate Frame is illustrated in Figure 3.

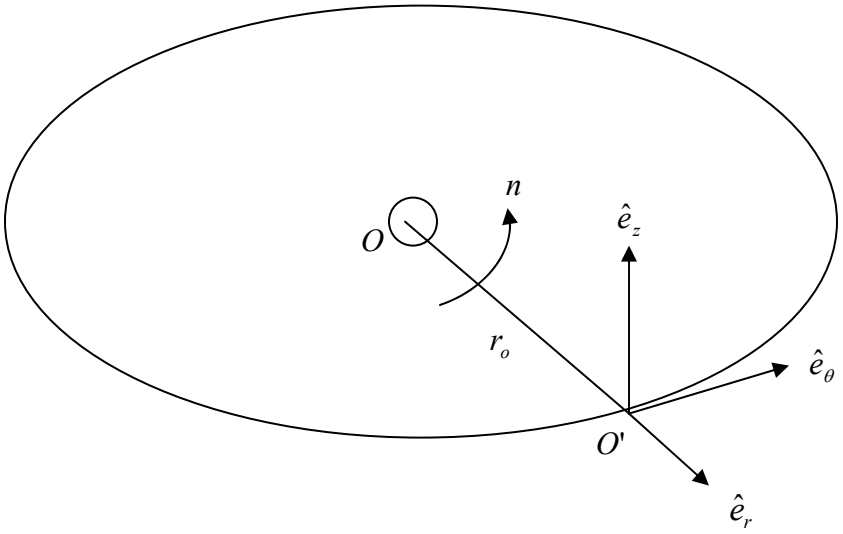

Figure 3 Hill's (RTZ) Coordinate Frame

It is important to be able to transform vectors from one coordinate frame to another. This can be done by finding a transformation matrix. This matrix can be multiplied by a vector in one coordinate frame to find its components in another frame. Since the Perifocal frame and Hill's frame are both in the same orbital plane, the transformation matrix need only account for rotation about one axis. For example, to transform a velocity vector from the RTZ frame to the PQW frame, the transformation matrix, *S*, is shown in Equation 1, where ν is the angle between the $\hat{p}$ axis and the $\hat{e}_r$ axis.

$$\left[\vec{v}_{pqw}\right] = \begin{bmatrix} v_{\hat{p}} \\ v_{\hat{q}} \\ v_{\hat{w}} \end{bmatrix} = \begin{bmatrix} \cos\nu & -\sin\nu & 0 \\ \sin\nu & \cos\nu & 0 \\ 0 & 0 & 1 \end{bmatrix} \begin{bmatrix} v_{\hat{r}} \\ v_{\hat{\theta}} \\ v_{\hat{z}} \end{bmatrix} = S\left[\vec{v}_{r\theta z}\right] \tag{1}$$

This case is illustrated in Figure 4, where $\hat{w}$ and $\hat{e}_z$ are collinear, out of the page.

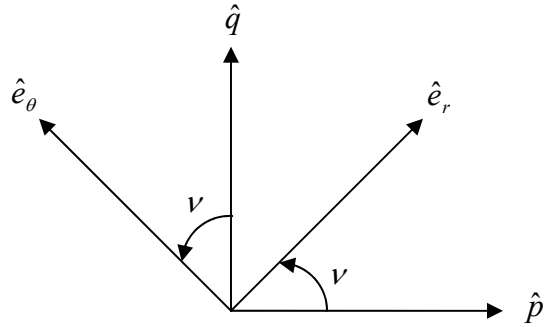

Figure 4 Transformation From RTZ to PQW Coordinate Frame

Transforming a vector from the PQW frame to the ECI frame can include up to three rotations, involving the right ascension of the ascending node, Ω, the argument of perigee, ω, and the inclination, *i*. The three rotation matrices are combined to give a single transformation matrix, *R*:

$$R = \begin{bmatrix} \cos\Omega\cos\omega - \sin\Omega(\cos i)\sin\omega & -\cos\Omega\sin\omega - \sin\Omega(\cos i)\cos\omega & \sin\Omega(\sin i) \\ \sin\Omega\cos\omega + \cos\Omega(\cos i)\sin\omega & -\sin\Omega\sin\omega + \cos\Omega(\cos i)\cos\omega & -\cos\Omega(\sin i) \\ (\sin i)\sin\omega & (\sin i)\cos\omega & (\cos i) \end{bmatrix} \quad (2)$$

which is multiplied by a vector in the PQW frame to find its components in the ECI frame. Equation 3 shows an example for transforming a position vector. (9)

$$[\vec{r}_{ijk}] = R[\vec{r}_{pqw}] \quad (3)$$

To transform a vector from the ECI frame to the PQW frame, the inverse of the transformation matrix is used, such as in Equation 4.

$$[\vec{r}_{pqw}] = R^{-1}[\vec{r}_{ijk}] \tag{4}$$

Similarly, a vector can be transformed from the PQW frame to the RTZ frame by using the inverse of the *S* transformation matrix:

$$[\vec{v}_{r\theta z}] = S^{-1}[\vec{v}_{pqw}] \tag{5}$$

Orbit Characterization

If the Earth is considered to be inertially fixed in space, a satellite in orbit around the Earth has six degrees of freedom. Therefore, specifying six orbital parameters completely defines the orbit. Two sets of parameters that can be used are the three dimensional position $(\vec{r})$ and velocity $(\vec{v})$, or the classical orbital elements (COE), which are identified in Table 1. (12)

Classical Orbital Elements	
a	Semi-Major Axis
e	Eccentricity
ν	True Anomaly
i	Inclination
Ω	Right Ascension of the Ascending Node
ω	Argument of Perigee

Table 1 Classical Orbital Elements

Both sets of parameters are used in this project, and it is convenient to be able to transform from one set to the other. To transform from the position and velocity vectors to COEs, the first step is to calculate the angular momentum, $\vec{H}$:

$$\vec{H} = \vec{r} \times \vec{v} \tag{6}$$

Next, the eccentricity can be found:

$$\vec{e} = \frac{\vec{v} \times \vec{H}}{\mu} - \frac{\vec{r}}{|\vec{r}|} \tag{7}$$

where μ is the Earth's gravitational parameter ($\mu = 398601\ km^3/s^2$). (12) The semi-major axis can be calculated with Equation 8.

$$a = \frac{|\vec{H}|^2}{\mu\left(1 - |\vec{e}|^2\right)} \tag{8}$$

The inclination is a function of the angular momentum and the unit vector, $\hat{k}$, where $\hat{k} = [0 \quad 0 \quad 1]$:

$$i = \cos^{-1}\left(\frac{\hat{k} \bullet \vec{H}}{|\vec{H}|}\right) \tag{9}$$

Next, a unit vector, $\hat{n}$, is found in the direction of the ascending node:

$$\hat{n} = \frac{\hat{k} \times \vec{H}}{|\hat{k} \times \vec{H}|} \tag{10}$$

The right ascension of the ascending node can now be calculated with Equation 11, and a quadrant check performed:

$$\Omega = \cos^{-1}\left(\hat{n} \bullet \hat{i}\right) \tag{11}$$

$$\begin{aligned} \left(\hat{n} \bullet \hat{j}\right) &\geq 0 \qquad 0 \leq \Omega \leq \pi \\ \left(\hat{n} \bullet \hat{j}\right) &< 0 \qquad \pi \leq \Omega \leq 2\pi \end{aligned}$$

The argument of perigee is found from Equation 12, and also requires a quadrant check:

$$\omega = \cos^{-1}\left(\frac{\hat{n} \bullet \vec{e}}{|\vec{e}|}\right) \tag{12}$$

$$\begin{aligned} \left(\vec{e} \bullet \hat{k}\right) &\geq 0 \qquad 0 \leq \omega \leq \pi \\ \left(\vec{e} \bullet \hat{k}\right) &< 0 \qquad \pi \leq \omega \leq 2\pi \end{aligned}$$

Finally, the true anomaly can be calculated, along with a quadrant check:

$$\nu = \cos^{-1}\left(\frac{\hat{n} \bullet \vec{r}}{|\vec{r}|}\right) \tag{13}$$

$$\begin{aligned} (\hat{n} \bullet \vec{v}) &\leq 0 \qquad 0 \leq \nu \leq \pi \\ (\hat{n} \bullet \vec{v}) &> 0 \qquad \pi \leq \nu \leq 2\pi \end{aligned}$$

To transform from COEs to the position and velocity vectors, the magnitude of the position and velocity are found using Equation 14 and Equation 15:

$$|\vec{r}| = \frac{a\left(1 - |\vec{e}|^2\right)}{1 + |\vec{e}|\cos\nu} \tag{14}$$

$$|\vec{v}| = \sqrt{\frac{U}{a\left(1 - |\vec{e}|^2\right)}} \tag{15}$$

Next, the position and velocity vectors are found in the PQW frame as follows:

$$\vec{r}_{pqw} = \begin{bmatrix} |\vec{r}|\cos\nu \\ |\vec{r}|\sin\nu \\ 0 \end{bmatrix} \tag{16}$$

$$\vec{v}_{pqw} = \begin{bmatrix} |\vec{v}|(-\sin\nu) \\ |\vec{v}|(|\vec{e}| + \cos\nu) \\ 0 \end{bmatrix} \tag{17}$$

The position and velocity can now be transformed into the ECI frame using Equation 2 and Equation 3.

Two-Body Motion

Satellite motion can be described by the two-body equations of motion, where the satellite and the Earth are the two bodies of interest. The origin in Figure 5 is inertially fixed, $\vec{R}_E$ is the position of the Earth relative to the origin, $\vec{R}_S$ is the position of the satellite relative to the origin, and $\vec{r}$ is the position of the satellite relative to the Earth. (9)

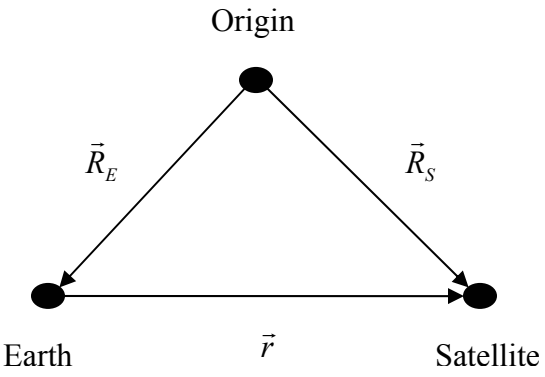

Figure 5 Two-Body Motion

$\vec{r}$ can be found from $\vec{R}_E$ and $\vec{R}_S$ through the following relation:

$$\vec{r} = \vec{R}_S - \vec{R}_E \tag{18}$$

Differentiating Equation 1 twice yields:

$$\ddot{\vec{r}} = \ddot{\vec{R}}_S - \ddot{\vec{R}}_E \tag{19}$$

Next, the forces on the satellite can be summed:

$$\Sigma \vec{F}_S = m_S \vec{a} = m_S \ddot{\vec{R}}_S \tag{20}$$

The only force acting on the satellite is the Earth's gravity:

$$\vec{F}_S = -\frac{G m_S m_E}{\left|\vec{R}_S - \vec{R}_E\right|^2} \hat{u} \tag{21}$$

where m_s and m_e are the mass of the satellite and the mass of the Earth, respectively, and *G* is the universal gravitational constant. The unit vector is defined as:

$$\hat{u} = \frac{\vec{R}_S - \vec{R}_E}{\left|\vec{R}_S - \vec{R}_E\right|} \tag{22}$$

Equating Equation 20 and Equation 21:

$$m_S \ddot{\vec{R}}_S = -\frac{G m_S m_E}{\left|\vec{R}_S - \vec{R}_E\right|^2} \hat{u} \tag{23}$$

Substituting Equation 22 into Equation 23:

$$m_S \ddot{\vec{R}}_S = -\frac{G m_S m_E}{\left|\vec{R}_S - \vec{R}_E\right|^3} (\vec{R}_S - \vec{R}_E) \tag{24}$$

and dividing through by m_s yields the satellite's acceleration with respect to the orgin:

$$\ddot{\vec{R}}_S = -\frac{G m_E}{\left|\vec{R}_S - \vec{R}_E\right|^3} (\vec{R}_S - \vec{R}_E) \tag{25}$$

Similar treatment for the Earth yields:

$$\ddot{\vec{R}}_E = \frac{Gm_S}{\left|\vec{R}_S - \vec{R}_E\right|^3}(\vec{R}_S - \vec{R}_E) \tag{26}$$

Substituting Equation 25 and Equation 26 into Equation 19:

$$\ddot{\vec{r}} = -\frac{G(m_S + m_E)}{\left|\vec{R}_S - \vec{R}_E\right|^3}(\vec{R}_S - \vec{R}_E) \tag{27}$$

Assuming $m_s << m_e$, let:

$$G(m_S + m_E) \approx Gm_E = \mu \tag{28}$$

Where μ is the Earth's gravitational parameter ($\mu = 398601\ km^3/s^2$). Finally:

$$\ddot{\vec{r}} = -\frac{\mu\vec{r}}{\left|\vec{r}\right|^3} \tag{29}$$

Perturbations

Equation 29 describes two-body motion without any other effects present, such as Earth oblateness, atmospheric drag, third body effects, or solar wind. Adding a perturbation term to Equation 29 yields:

$$\ddot{\vec{r}} = -\frac{\mu\vec{r}}{\left|\vec{r}\right|^3} + \vec{a}_p \tag{30}$$

For this project, the J_2 and drag perturbations will be the only ones considered:

$$\vec{a}_p = \vec{a}_{J2} + \vec{a}_D \tag{31}$$

Earth Oblateness

The Earth is not a perfect sphere; rotational motion causes it to bulge about the equator. The uneven mass distribution produces a non-uniform gravity field, which causes periodic affects to a satellite's orbital elements. Additionally, the Right Ascension of the Ascending Node, Ω, and the argument of perigee, ω, experience secular affects. These effects can be modeled using potential theory. (1)

Expanding $\vec{r}$ into its constituent x, y, z components in the $\hat{i}$, $\hat{j}$, $\hat{k}$ directions:

$$\ddot{\vec{r}} = \left[\frac{-\mu x}{\left(x^2+y^2+z^2\right)^{\frac{3}{2}}} + \vec{a}_{J_2 i}\right]\hat{i} + \left[\frac{-\mu y}{\left(x^2+y^2+z^2\right)^{\frac{3}{2}}} + \vec{a}_{J_2 j}\right]\hat{j} + \left[\frac{-\mu z}{\left(x^2+y^2+z^2\right)^{\frac{3}{2}}} + \vec{a}_{J_2 k}\right]\hat{k} \tag{32}$$

Next, let B be a potential function, such that

$$\nabla B = \vec{a}_{J_2} \tag{33}$$

Therefore,

$$\frac{\partial}{\partial x}\left(\frac{\mu}{|\vec{r}|} + B\right) = \left[\frac{-\mu x}{(x^2+y^2+z^2)^{\frac{3}{2}}} + \vec{a}_{J_2 i}\right] \tag{34}$$

$$\frac{\partial}{\partial y}\left(\frac{\mu}{|\vec{r}|} + B\right) = \left[\frac{-\mu y}{(x^2+y^2+z^2)^{\frac{3}{2}}} + \vec{a}_{J_2 j}\right] \tag{35}$$

$$\frac{\partial}{\partial z}\left(\frac{\mu}{|\vec{r}|} + B\right) = \left[\frac{-\mu z}{(x^2+y^2+z^2)^{\frac{3}{2}}} + \vec{a}_{J_2 k}\right] \tag{36}$$

Comparing Equations 34, 35, and 36 with 32, it can be seen that

$$\ddot{\vec{r}} = \nabla\left(\frac{\mu}{|\vec{r}|} + B\right) \tag{37}$$

where B is an infinite series that models the Earth's non-homogeneous mass distribution:

$$B = \frac{-\mu}{|\vec{r}|}\left\{\sum_{n=2}^{\infty}\left[\left(\frac{R_e}{|\vec{r}|}\right)^n J_n P_n(\sin\phi) + \sum_{m=1}^{n}\left(\frac{R_e}{|\vec{r}|}\right)^n (C_{nm}\cos\varphi + S_{nm}\sin\varphi) P_{nm}(\sin\phi)\right]\right\} \tag{38}$$

and $\varphi = m\lambda$, R_e is the Earth's radius at the equator ($R_e = 6378.135\ km$), ϕ is the latitude measured from the equator, $|\vec{r}|$ is the magnitude of the satellite's position vector, J_n, C_{nm} and S_{nm} are the zonal, tesseral and sectorial harmonic coefficients, respectively, and P_n and P_{nm} are Legendre polynomials. (2)

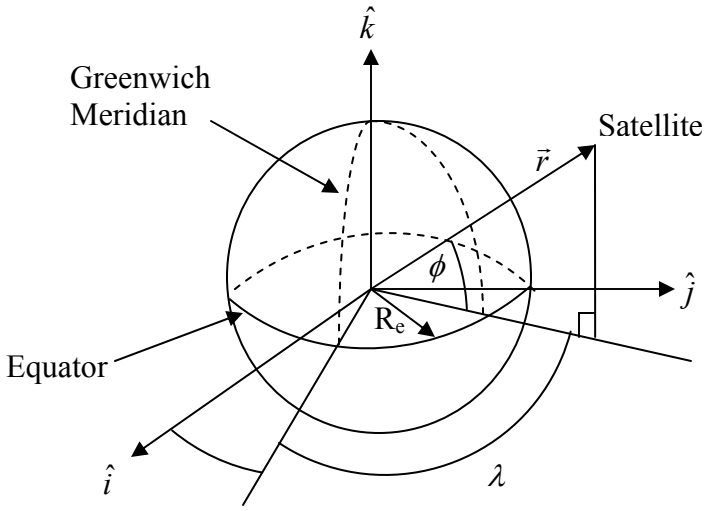

Figure 6 Geocentric Spherical Coordinate Frame

The Earth's oblateness has a zonal harmonic effect, symmetric about the Earth's axis of rotation and independent of longitude. The J_2 contribution is much larger than that of other harmonic coefficients, and will therefore be the only one included here. Reducing Equation 38 and considering only the case when $n = 2$ yields:

$$B = \frac{-\mu}{|\vec{r}|}\left(\frac{R_e}{|\vec{r}|}\right)^2 J_2 P_2(\sin\phi) \tag{39}$$

where $J_2 = 0.0010826$ and the second Legendre polynomial is

$$P_2(\sin\phi) = \frac{1}{2}\left(3(\sin\phi)^2 - 1\right) \tag{40}$$

Substituting Equation 40 into Equation 39 and rearranging:

$$B = \frac{\mu J_2 {R_e}^2}{2|\vec{r}|^3}\left[1 - 3(\sin\phi)^2\right] \tag{41}$$

From the geometry in Figure 6:

$$\sin\phi = \frac{z}{|\vec{r}|} \tag{42}$$

Substituting Equation 42 into Equation 41:

$$B = \frac{\mu J_2 {R_e}^2}{2|\vec{r}|^3}\left(1 - 3\frac{z^2}{|\vec{r}|^2}\right) = \frac{\mu J_2 {R_e}^2}{2}\left(\frac{|\vec{r}|^2 - 3z^2}{|\vec{r}|^5}\right) \tag{43}$$

taking the gradient:

$$\vec{a}_{J_2} = \nabla B = \begin{bmatrix} \frac{\partial}{\partial x} B \\ \frac{\partial}{\partial y} B \\ \frac{\partial}{\partial z} B \end{bmatrix} = \frac{\mu J_2 R_e^{\,2}}{2} \begin{bmatrix} \frac{|\vec{r}|^5 \left(2|\vec{r}| \frac{x}{|\vec{r}|} \right) - \left(-3z^2 + |\vec{r}|^2 \right) 5|\vec{r}|^4 \frac{x}{|\vec{r}|}}{|\vec{r}|^{10}} \\ \frac{|\vec{r}|^5 \left(2|\vec{r}| \frac{y}{|\vec{r}|} \right) - \left(-3z^2 + |\vec{r}|^2 \right) 5|\vec{r}|^4 \frac{y}{|\vec{r}|}}{|\vec{r}|^{10}} \\ \frac{|\vec{r}|^5 \left(-6z + 2|\vec{r}| \frac{z}{|\vec{r}|} \right) - \left(-3z^2 + |\vec{r}|^2 \right) 5|\vec{r}|^4 \frac{z}{|\vec{r}|}}{|\vec{r}|^{10}} \end{bmatrix} \tag{44}$$

and simplifying:

$$\vec{a}_{J_2} = \frac{\mu J_2 R_e^{\,2}}{2} \begin{bmatrix} \left(\frac{15z^2}{|\vec{r}|^7} \right) x - \left(\frac{3}{|\vec{r}|^5} \right) x \\ \left(\frac{15z^2}{|\vec{r}|^7} \right) y - \left(\frac{3}{|\vec{r}|^5} \right) y \\ \left(\frac{15z^2}{|\vec{r}|^7} \right) z - \left(\frac{3}{|\vec{r}|^5} \right) 3z \end{bmatrix} \tag{45}$$

Drag

Atmospheric drag can alter the orbit of a satellite below about 1000 km in altitude. The drag acceleration is added to the two-body equations of motion as a second component of the perturbation term, as shown in Equation 31. The drag acceleration is calculated as follows:

$$\vec{a}_D = -\frac{1}{2}\rho\left|\vec{V}\right|^2 \frac{C_D A}{m}\hat{i}_v \tag{46}$$

where ρ is atmospheric density, $\left|\vec{V}\right|$ is the magnitude of the velocity vector, C_D is the drag coefficient, A is the satellite cross-sectional area presented to the atmosphere, m is the mass of the satellite, and $\hat{i}_v$ is a unit vector in the direction of the velocity vector. (1)

The density, ρ, is calculated using the following equation and a standard atmosphere:

$$\rho = \rho_o e^{-\left[\frac{(h-h_o)}{H}\right]} \tag{47}$$

where ρ_o is the density at a reference altitude, h is the current altitude, h_o is the reference altitude, and H is the scale height for the reference altitude. (10)

The drag coefficient, C_D, usually ranges from 2.2 for a sphere to 3.0 for a cylinder. (1) For this project, the drag coefficient for the target satellite was set at 2.2 and for the microsatellite it was set at 3.0. This represents a worst-case scenario for the microsatellite's drag coefficient.

For the target satellite, the cross-sectional area was set at 4.2 m^2 and the mass was entered as 725 kg. These parameters correspond to Defense Meterological Satellite Program (DMSP) satellites. They were selected as representative of an operational satellite, although DMSP satellites orbit at higher altitude than the target satellite used in this project. (5)

A mass of 100 kg and a cross-sectional area of 1.5 m^2 were used for the microsatellite. The mass was selected based on the definition of a microsatellite, and the relatively large cross-sectional area was used to represent worst-case performance.

Relative Motion

For rendezvous maneuvers, it is useful to know the positions and velocities of the microsatellite and the target relative to a circular reference frame. In Figure 7, O is the origin centered in the Earth and fixed in inertial space. O' is the origin of a reference frame that is centered on the instantaneous location of a point moving about O in a circular orbit with mean motion, n. The unit vectors in the circular reference frame are $\hat{e}_r, \hat{e}_\theta, \hat{e}_z$ in the radial, in-track, and out of plane directions, respectively, and r_o is the radius of the circular reference orbit. To find the equations for relative motion, the left side of Equation 29 is found by taking the second derivative of position, and the right side of Equation 29 is found by expanding terms. Then, the two sides are equated. (9)

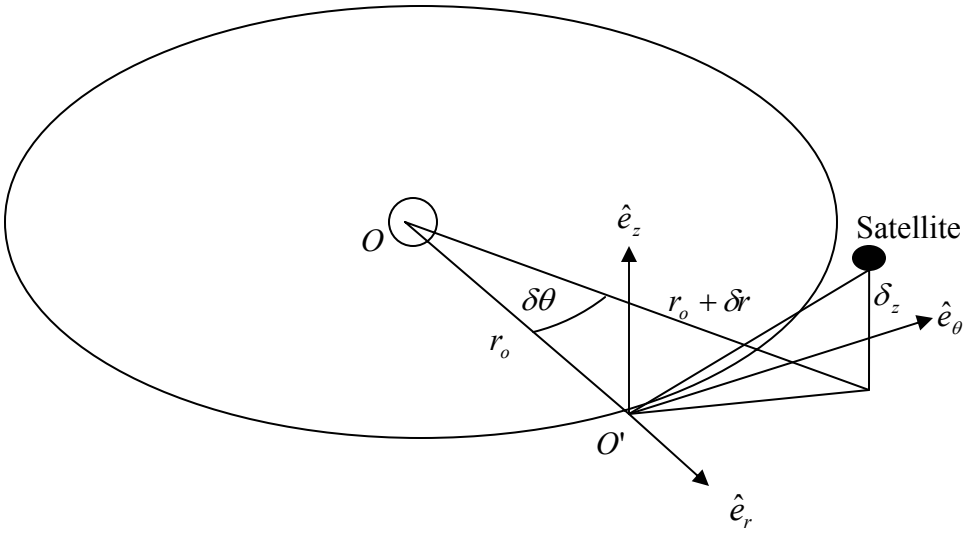

Figure 7 Hill's Coordinates

In this frame, the position of the satellite is:

$$\vec{r} = \left[(r_o + \delta r)\cos\delta\theta\right]\hat{e}_r + \left[(r_o + \delta r)\sin\delta\theta\right]\hat{e}_\theta + \left[\delta z\right]\hat{e}_z \tag{48}$$

and the velocity can be found from:

$$\vec{v} = {}^{i}\frac{d}{dt}(\vec{r}) = {}^{o}\frac{d}{dt}(\vec{r}) + (\vec{n}\times\vec{r}) \tag{49}$$

where the superscripts i and o correspond to the inertial and circular reference frames, respectively, and the mean motion of the circular reference frame is:

$$\vec{n} = \sqrt{\frac{\mu}{r_o^{\,3}}}\hat{e}_z \tag{50}$$

Applying Equation 49:

$$\begin{aligned}\vec{v} = &\left[\delta\dot{\theta} r_o(-\sin\delta\theta) + \delta\dot{r}(\cos\delta\theta) - \delta r(\sin\delta\theta)\delta\dot{\theta}\right]\hat{e}_r \\ &+ \left[r_o(\cos\delta\theta)\delta\dot{\theta} + \delta\dot{r}(\sin\delta\theta) + \delta r\delta\dot{\theta}(\cos\delta\theta)\right]\hat{e}_\theta \\ &+ \left[\delta\dot{z}\right]\hat{e}_z \\ &+ (n\hat{e}_z)\times\{\left[(r_o+\delta r)\cos\delta\theta\right]\hat{e}_r + \left[(r_o+\delta r)\sin\delta\theta\right]\hat{e}_\theta + \left[\delta z\right]\hat{e}_z\}\end{aligned} \tag{51}$$

combining terms:

$$\vec{v} = \left[\delta\dot{r}\cos\delta\theta - \left(\delta\dot{\theta}+n\right)(r_o+\delta r)\sin\delta\theta\right]\hat{e}_r + \left[\left(\delta\dot{\theta}+n\right)(r_o+\delta r)\cos\delta\theta + \delta\dot{r}\sin\delta\theta\right]\hat{e}_\theta + \left[\delta\dot{z}\right]\hat{e}_z \tag{52}$$

The position (Equation 48) and velocity (Equation 52) in the relative frame can now be linearized by assuming δr, $\delta\theta$, δz, $\delta\dot{r}$, $\delta\dot{\theta}$ and $\delta\dot{z}$ are small. Canceling higher order terms, and using the small angle approximations $\cos\delta\theta \approx 1$ and $\sin\delta\theta \approx \delta\theta$ yields:

$$\vec{r} \approx (r_o+\delta r)\hat{e}_r + (r_o\delta\theta)\hat{e}_\theta + (\delta z)\hat{e}_z \tag{53}$$

$$\vec{v} \approx \left(\delta\dot{r} - nr_o\delta\theta\right)\hat{e}_r + \left[r_o\delta\dot{\theta} + n(r_o+\delta r)\right]\hat{e}_\theta + (\delta\dot{z})\hat{e}_z \tag{54}$$

Now, taking the derivative of velocity yields the linearized acceleration:

$$\vec{a} = {}^{i}\frac{d}{dt}(\vec{v}) = {}^{o}\frac{d}{dt}(\vec{v}) + (\vec{n}\times\vec{v}) \tag{55}$$

$$\vec{a} = \left(\delta\ddot{r} - nr_o\delta\dot{\theta}\right)\hat{e}_r + \left(r_o\delta\ddot{\theta} + n\delta\dot{r}\right)\hat{e}_\theta + (\delta\ddot{z})\hat{e}_z - \left(nr_o\delta\dot{\theta} + n^2(r_o+\delta r)\right)\hat{e}_r + \left(n\delta\dot{r} - n^2 r_o\delta\theta\right)\hat{e}_\theta \tag{56}$$

combining terms:

$$\vec{a} = \ddot{\vec{r}} = \left[\delta\ddot{r} - 2nr_o\delta\dot{\theta} - n^2(r_o+\delta r)\right]\hat{e}_r + \left(r_o\delta\ddot{\theta} + 2n\delta\dot{r} - n^2 r_o\delta\theta\right)\hat{e}_\theta + (\delta\ddot{z})\hat{e}_z \tag{57}$$

Equation 57 represents the left side of Equation 29. To find the expression for the right side of the equation in the relative frame, the terms are expanded using the linearized position vector (Equation 53). In the denominator:

$$\left|\vec{r}\right|^3 = \left(\sqrt{\left(r_o+\delta r\right)^2+\left(r_o\delta\theta\right)^2+\left(\delta z\right)^2}\right)^3 = \left({r_o}^2+2r_o\delta r+\delta r^2+{r_o}^2\delta\theta^2+\delta z^2\right)^{\frac{3}{2}}$$
$$= \left({r_o}^2\left[1+2\frac{\delta r}{r_o}+\frac{\delta r^2}{{r_o}^2}+\delta\theta^2+\frac{\delta z^2}{{r_o}^2}\right]\right)^{\frac{3}{2}} = \left(r_o\right)^3\left(1+2\frac{\delta r}{r_o}+\frac{\delta r^2}{{r_o}^2}+\delta\theta^2+\frac{\delta z^2}{{r_o}^2}\right)^{\frac{3}{2}} \quad (58)$$

Therefore:

$$-\frac{\mu\vec{r}}{\left|\vec{r}\right|^3} = -\left(\frac{\mu}{{r_o}^3}\right)\frac{\left[\left(r_o+\delta r\right)\hat{e}_r+\left(r_o\delta\theta\right)\hat{e}_\theta+\left(\delta z\right)\hat{e}_z\right]}{\left(1+2\frac{\delta r}{r_o}+\frac{\delta r^2}{{r_o}^2}+\delta\theta^2+\frac{\delta z^2}{{r_o}^2}\right)^{\frac{3}{2}}} \quad (59)$$

A binomial expansion can be used for the denominator: (3)

$$\frac{1}{\left(1+2\frac{\delta r}{r_o}+\frac{\delta r^2}{{r_o}^2}+\delta\theta^2+\frac{\delta z^2}{{r_o}^2}\right)^{\frac{3}{2}}} = \left[1-\frac{3}{2}\left(2\frac{\delta r}{r_o}+\frac{\delta r^2}{{r_o}^2}+\delta\theta^2+\frac{\delta z^2}{{r_o}^2}\right)\right.$$
$$\left.+\frac{15}{8}\left(2\frac{\delta r}{r_o}+\frac{\delta r^2}{{r_o}^2}+\delta\theta^2+\frac{\delta z^2}{{r_o}^2}\right)^2+\textit{Higher Order Terms}\right] \quad (60)$$

It can be seen that the second order and higher terms will not be linear, and will therefore be cancelled. This yields:

$$\frac{1}{\left(1+2\frac{\delta r}{r_o}+\frac{\delta r^2}{{r_o}^2}+\delta\theta^2+\frac{\delta z^2}{{r_o}^2}\right)^{\frac{3}{2}}} = \left[1-3\frac{\delta r}{r_o}\right] \quad (61)$$

Recognizing the magnitude of the mean motion from Equation 32 and substituting Equation 61 into Equation 59:

$$-\frac{\mu}{\left|\vec{r}\right|^3} = -n^2\left[\left(r_o+\delta r\right)\hat{e}_r+\left(r_o\delta\theta\right)\hat{e}_\theta+\left(\delta z\right)\hat{e}_z\right]\left[1-3\frac{\delta r}{r_o}\right] \quad (62)$$

Multiplying and again eliminating higher terms produces the final result for the right side of Equation 29:

$$-\frac{\mu}{\left|\vec{r}\right|^3} = -n^2\left[\left(r_o - 2\delta r\right)\hat{e}_r + \left(r_o\delta\theta\right)\hat{e}_\theta + \left(\delta z\right)\hat{e}_z\right] \tag{63}$$

Equation 57 and Equation 63 can now be equated:

$$\begin{aligned} \delta\ddot{r} - 2nr_o\delta\dot{\theta} - n^2\left(r_o + \delta r\right) &= -n^2\left(r_o - 2\delta r\right) \\ r_o\delta\ddot{\theta} + 2n\delta\dot{r} - n^2 r_o\delta\theta &= -n^2 r_o\delta\theta \\ \delta\ddot{z} &= -n^2\delta z \end{aligned} \tag{64}$$

Solving Equation 64 yields:

$$\begin{aligned} \begin{bmatrix} \delta r(t) \\ r_o\delta\theta(t) \\ \delta z(t) \end{bmatrix} &= \begin{bmatrix} 3n\sin\psi & 0 & 0 \\ 6n\left(\cos\psi - 1\right) & 0 & 0 \\ 0 & 0 & -n\sin\psi \end{bmatrix}\begin{bmatrix} \delta r(0) \\ r_o\delta\theta(0) \\ \delta z(0) \end{bmatrix} \\ &+ \begin{bmatrix} \cos\psi & 2\sin\psi & 0 \\ -2\sin\psi & 4\cos\psi - 3 & 0 \\ 0 & 0 & \cos\psi \end{bmatrix}\begin{bmatrix} \delta\dot{r}(0) \\ r_o\delta\dot{\theta}(0) \\ \delta\dot{z}(0) \end{bmatrix} \end{aligned} \tag{65}$$

and:

$$\begin{aligned} \begin{bmatrix} \delta r(t) \\ r_o\delta\theta(t) \\ \delta z(t) \end{bmatrix} &= \begin{bmatrix} 4 - 3\cos\psi & 0 & 0 \\ 6\left(\sin\psi - \psi\right) & 1 & 0 \\ 0 & 0 & \cos\psi \end{bmatrix}\begin{bmatrix} \delta r(0) \\ r_o\delta\theta(0) \\ \delta z(0) \end{bmatrix} \\ &+ \begin{bmatrix} \dfrac{\sin\psi}{n} & \dfrac{2 - 2\cos\psi}{n} & 0 \\ \dfrac{2\cos\psi - 2}{n} & \dfrac{4\sin\psi - 3\psi}{n} & 0 \\ 0 & 0 & \dfrac{\sin\psi}{n} \end{bmatrix}\begin{bmatrix} \delta\dot{r}(0) \\ r_o\delta\dot{\theta}(0) \\ \delta\dot{z}(0) \end{bmatrix} \end{aligned} \tag{66}$$

where $\psi = nt$. In compact notation:

$$\left[\delta\vec{v}(t)\right] = \Phi_{vr}\left[\delta\vec{r}(0)\right] + \Phi_{vv}\left[\delta\vec{v}(0)\right] \tag{67}$$

and:

$$\left[\delta\vec{r}(t)\right] = \Phi_{rr}\left[\delta\vec{r}(0)\right] + \Phi_{rv}\left[\delta\vec{v}(0)\right] \tag{68}$$

These equations are only valid when δr and δz are small, although $r_o\delta\theta$ can be large.

III. Control

Both of the control methodologies evaluated in this thesis are based on linear equations of motion, yet the orbits are propagated using non-linear equations. The linear equations are only valid near a circular orbit, and normally are used with a leader satellite in a perfectly circular orbit. The follower satellite remains "close" to the leader, and its position and velocity are found relative to the leader satellite. The equations are linearized about a circular lead orbit, so the lead satellite's orbit must be circular for proper application of the equations. For this project, it was decided to allow the target satellite to have some eccentricity in its nominal orbit. The microsatellite will have eccentricity introduced into its orbit as the control solutions are applied. To allow for both satellites to have non-zero eccentricity, and to still comply with the requirement for the leader satellite to be in a perfectly circular orbit, it was decided to use a "virtual" leader. The virtual leader orbit is constructed to have an initial position vector that is collinear with the target satellite, to be in a coplanar orbit with the target satellite, to have the same semi-major axis length and therefore the same period as the target, but to have zero eccentricity. The virtual reference orbit will therefore remain close to the target satellite throughout its orbit. The position and velocity of the target and the microsatellite are found relative to the virtual circular reference orbit. Instead of effecting rendezvous to the origin of the relative circular reference frame, the microsatellite is able to pursue the target satellite which is moving with respect to the reference frame. (12)

For both of the control methods considered, it is necessary to find the position and velocity of a satellite relative to the circular reference frame. First, the position and velocity are transformed into the circular reference orbit's PQW coordinate frame. Then the true anomaly of the reference orbit can be found from the *p* and *q* components of the reference's position vector. Using MATLAB's *atan2* function ensures quadrant accuracy:

$$\nu = atan2\left(\frac{r_q}{r_p}\right)_{ref} \tag{69}$$

The true anomaly can then be used to set up a transformation matrix, *S*, which is used to transform the satellite's position from the circular reference's PQW coordinate frame to its RTZ coordinate frame.

$$(\vec{r}_{rθz})_{satellite} = S(\vec{r}_{pqw})_{satellite} \tag{70}$$

The *atan2* function can now be used to find $\delta\theta$ without quadrant ambiguity:

$$\delta\theta = atan2\left(\frac{r_\theta}{r_r}\right)_{satellite} \tag{71}$$

The position vector of the satellite relative to the circular reference orbit is calculated as follows:

$$\delta\vec{r} = \begin{bmatrix} \left(\sqrt{r_r^{\,2} + r_\theta^{\,2}}\right)_{satellite} - \left(\sqrt{r_r^{\,2} + r_\theta^{\,2}}\right)_{ref} \\ r_o\delta\theta \\ (r_z)_{satellite} - (r_z)_{ref} \end{bmatrix} \tag{72}$$

To find the relative velocity vector, it is useful to find the angle between the reference orbit's *p* axis and the satellite's position vector in the *pq* plane.

$$\gamma = atan2\left(\frac{r_q}{r_p}\right)_{satellite} \tag{73}$$

This angle can be used to build a transformation matrix, *T*, which will be used to find the radial, tangential, and out-of-plane components of the velocity vector:

$$\left(\vec{v}_{123}\right)_{satellite} = T\left(\vec{v}_{pqw}\right)_{satellite} \tag{74}$$

Next, the magnitude of the satellite's angular velocity can be found:

$$\left|\dot{\vec{\theta}}\right| = \frac{\left|\left(\vec{v}_2\right)_{satellite}\right|}{\left|\vec{r}\right|} \tag{75}$$

Finally, the relative velocity can be found:

$$\delta\vec{v} = \begin{bmatrix} \left(\vec{v}_1\right)_{satellite} \\ r_o\left(\left|\dot{\vec{\theta}}\right| - n\right) \\ \left(\vec{v}_3\right)_{satellite} \end{bmatrix} \tag{76}$$

where *n* is the mean motion of the circular reference orbit.

Clohessey-Wiltshire

The first control methodology considered for this project utilizes the Clohessey-Wiltshire (CW) equations. This technique produces an impulsive control thrust which initiates the rendezvous. A second impulsive thrust is applied once rendezvous is complete, to null out the relative velocity between the microsatellite and the target satellite.

Equation 68 is rearranged to solve for the relative velocity needed at time $t = 0$ in order to achieve rendezvous at a specified time, $t = T$:

$$[\delta\vec{v}(0)] = \Phi_{rv}^{-1}([\delta\vec{r}(T)] - \Phi_{rr}[\delta\vec{r}(0)]) \tag{77}$$

To calculate the Δv required at time $t = 0$, the necessary inputs are the microsatellite's starting position relative to the circular reference, the desired rendezvous time, the desired position of the microsatellite relative to the circular reference at the rendezvous time, and the mean motion of the circular reference frame. (12)

The desired relative position for the microsatellite at the rendezvous time is the same as the position of the target satellite at the rendezvous time. The target's initial position and velocity relative to the circular reference frame can be found as described above, and then Equation 68 can be employed to find the target's position relative to the circular reference at the specified rendezvous time.

The microsatellite's initial position relative to the circular reference frame is also found using the procedure described earlier in this chapter. The mean motion of the circular reference frame is calculated using Equation 50. Once all of the input values are entered into Equation 77, the necessary relative velocity at time $t = 0$ can be calculated. Equation 52 is used to transform the velocity from the relative frame to an inertial frame. It is then transformed into the ECI frame and applied to the microsatellite, which is propagated using the non-linear equations of motion. To calculate the necessary Δv, the microsatellite's initial velocity is subtracted from the velocity calculated for rendezvous.

$$\Delta\vec{v} = \left(\vec{v}_{ijk}\right)_{calculated} - \left(\vec{v}_{ijk}\right)_{initial} \tag{78}$$

At the specified rendezvous time, a second impulsive thrust can be applied to null the relative velocity between the microsatellite and the target. This second $\Delta\vec{v}$ is added to the first to find the total $\Delta\vec{v}$ for the CW rendezvous.

The Clohessey Wiltshire equations can be improved by adding the J_2 perturbation to the calculation, which is discussed in the next section. Although drag was added to the equations of motion in the previous chapter, the drag perturbation is not accounted for in the Clohessey Wiltshire equations for this project.

Clohessey Wiltshire with J_2

McLaughlin, et al, discuss addition of the J_2 perturbation term to Hill's equations. (4) The primary change is substitution of $\omega_{r\theta}$ in place of n in the in-plane components $(\delta r, r_o \delta\theta)$ and ω_z in place of n in the out of plane component (δz) in the Φ matrices in Equation 66, where:

$$\omega_{r\theta} = n + \dot{M} \tag{79}$$

$$\omega_z = n + \dot{M} + \dot{\omega} \tag{80}$$

and:

$$\dot{M} = \frac{3nR_E{}^2 J_2 \sqrt{1-e^2}}{4p^2}\left(2 - 3\sin^2 i\right) \tag{81}$$

$$\dot{\omega} = \frac{3nR_E{}^2 J_2}{4p^2}\left(4 - 5\sin^2 i\right) \tag{82}$$

where $\dot{M}$ is the effect of J_2 on the mean anomaly, $\dot{\omega}$ is the effect of J_2 on the argument of perigee, n is the mean motion, R_E is the mean radius of the Earth at the equator, J_2 is the perturbation term, e is the eccentricity, i is the inclination and p is the semilatus rectum. (4)

Further terms are discussed by McLaughlin, et al, to account for the J_2 effects resulting from the target and chase satellites having different inclinations. However, the inclinations are assumed to be the same for this project, so the extra terms are not discussed here.

After $\omega_{r\theta}$ and ω_z are substituted into Equation 66, by replacing $\psi = nt$ with $\psi_{r\theta} = \omega_{r\theta} t$ in the in-plane components of the Φ matrices, and replacing $\psi = nt$ with $\psi_z = \omega_z t$ in the out of plane components of the Φ matrices, then Equation 66 can be rearranged into the form of Equation 77 to give a solution for the necessary velocity as discussed in the previous section.

Linear Quadratic Regulator

The second control methodology considered for this project was a Linear Quadratic Regulator (LQR). Again utilizing the relative reference frame (Figure 7) and the relative equations of motion (Equation 64), a vector comprising both the relative position and velocity can be defined: (2)

$$\vec{x} = \begin{bmatrix} \delta\ddot{r} \\ \delta r \\ r_o \delta\dot{\theta} \\ r_o \delta\theta \\ \delta\ddot{z} \\ \delta z \end{bmatrix} \tag{83}$$

and its derivative is:

$$\dot{\vec{x}} = \begin{bmatrix} \delta\ddot{r} \\ \delta\dot{r} \\ r_o\delta\ddot{\theta} \\ r_o\delta\dot{\theta} \\ \delta\ddot{z} \\ \delta\dot{z} \end{bmatrix} \tag{84}$$

The relative equations of motion can be placed in state equation form:

$$\dot{\vec{x}} = A\vec{x} + B\vec{u} \tag{85}$$

where $\vec{u}$ is a vector of control inputs. Equations 64, 83 and 84 can now be used to write Equation 85 as:

$$\begin{bmatrix} \delta\ddot{r} \\ \delta\dot{r} \\ r_o\delta\ddot{\theta} \\ r_o\delta\dot{\theta} \\ \delta\ddot{z} \\ \delta\dot{z} \end{bmatrix} = \begin{bmatrix} 0 & 3n^2 & 2n & 0 & 0 & 0 \\ 1 & 0 & 0 & 0 & 0 & 0 \\ -2n & 0 & 0 & 0 & 0 & 0 \\ 0 & 0 & 1 & 0 & 0 & 0 \\ 0 & 0 & 0 & 0 & 0 & -n^2 \\ 0 & 0 & 0 & 0 & 1 & 0 \end{bmatrix} \begin{bmatrix} \delta\dot{r} \\ \delta r \\ r_o\delta\dot{\theta} \\ r_o\delta\theta \\ \delta\dot{z} \\ \delta z \end{bmatrix} + \begin{bmatrix} 1 & 0 & 0 \\ 0 & 0 & 0 \\ 0 & 1 & 0 \\ 0 & 0 & 0 \\ 0 & 0 & 1 \\ 0 & 0 & 0 \end{bmatrix} \begin{bmatrix} u_r \\ u_\theta \\ u_z \end{bmatrix} \tag{86}$$

A Linear Quadratic Regulator obtains the optimal gain matrix, K for the control vector: (6)

$$\vec{u} = -K\vec{x} \tag{87}$$

by minimizing the performance index:

$$J = \int_0^\infty \left(x'Qx + u'Ru\right)dt \tag{88}$$

The algebraic Riccati equation is solved to find S:

$$SA + A'S - SBR^{-1}B'S + Q = 0 \tag{89}$$

where Q is the state weighting matrix and R is the control weighting matrix. Higher values in the Q matrix speed movement toward the desired state, and higher values in the R matrix reduce control usage. For this project, Q and R will have the following forms:

$$Q = \begin{bmatrix} q & 0 & 0 & 0 & 0 & 0 \\ 0 & q & 0 & 0 & 0 & 0 \\ 0 & 0 & q & 0 & 0 & 0 \\ 0 & 0 & 0 & q & 0 & 0 \\ 0 & 0 & 0 & 0 & q & 0 \\ 0 & 0 & 0 & 0 & 0 & q \end{bmatrix} \tag{90}$$

$$R = \begin{bmatrix} r & 0 & 0 \\ 0 & r & 0 \\ 0 & 0 & r \end{bmatrix} \tag{91}$$

Finally, the optimal gain matrix is calculated:

$$K = R^{-1} B' S \tag{92}$$

For this project, the optimal gain matrix is found by entering the A, B, Q and R matrices into MATLAB's LQR function. Once calculated during a run, the gain matrix never needs to be recalculated.

For this project, the microsatellite is chasing the target satellite rather than the circular reference. Therefore, the control input is based on the difference between the microsatellite's state vector and the target's state vector (i.e., the error state):

$$\begin{bmatrix} u_r \\ u_\theta \\ u_z \end{bmatrix} = -K \begin{bmatrix} \delta\dot{r}_{micro} - \delta\dot{r}_{tgt} \\ \delta r_{micro} - \delta r_{tgt} \\ r_o \delta\dot{\theta}_{micro} - r_o \delta\dot{\theta}_{tgt} \\ r_o \delta\theta_{micro} - r_o \delta\theta_{tgt} \\ \delta\dot{z}_{micro} - \delta\dot{z}_{tgt} \\ \delta z_{micro} - \delta z_{tgt} \end{bmatrix} \tag{93}$$

The following steps are repeated during propagation. First, the position and velocity of the target and microsatellite are found relative to the circular reference. Then the control input is calculated using Equation 93. The control input, $\vec{u}$, is actually a specific thrust, so the calculated value is already in an inertial frame. It is then transformed into the ECI frame and added to the two-body equations of motion:

$$\ddot{\vec{r}} = -\frac{\mu \vec{r}}{\left|\vec{r}\right|^3} + \vec{a}_p + \vec{u} \tag{94}$$

The target, microsatellite and reference orbits are propagated one time step using numerical integration. The Δv for each step is calculated using Euler integration; the magnitude of the control acceleration is multiplied by the size of the time step and accumulated over the run.

The next iteration begins with finding the position and velocity of the target and microsatellite relative to the circular reference frame. The process is repeated until rendezvous is achieved. This algorithm is depicted in Appendix B.

IV. Results

The results in this chapter were obtained by starting with a target orbit having the initial orbital elements found in Table 2, unless otherwise specified.

Orbital Elements		Values	Units
a	Semi-Major Axis	6772.888912204840	kilometers
e	Eccentricity	0.00098877135498	dimensionless
ν	True Anomaly	0.79736386485827	radians
i	Inclination	0.90757990078380	radians
Ω	Right Ascension of the Ascending Node	1.51843760980691	radians
ω	Argument of Perigee	5.59054044657763	radians

Table 2 Initial Orbital Elements for the Target Orbit

The starting position of the microsatellite is $\delta\vec{r} = \begin{bmatrix} 0 & -1000 & 0 \end{bmatrix}$ unless otherwise specified.

Simulator Capability

Orbits based on the non-linear equations of motion are propagated for this project using numerical integration. The explicit Runge-Kutta 4,5 (Dormand, Prince pair) method is employed in MATLAB using the ODE45 command. For this project, the relative tolerance has been set to 2.2205e-14 and the absolute tolerance has been set to 1e-200. A tighter relative tolerance was found to be beyond the capability of the system.

With these tolerances set, a circular orbit was propagated ten revolutions using the non-linear equations of motion; the same orbit was propagated ten revolutions using the linear equations of motion. Since the circular orbit has no offsets from the identical circular reference orbit, the criteria for linearization are perfectly satisfied. However, when the relative position between the linear and non-linear solutions is compared, a small error is observed. This error is attributable to the precision of the simulator, and is depicted in Figure 8:

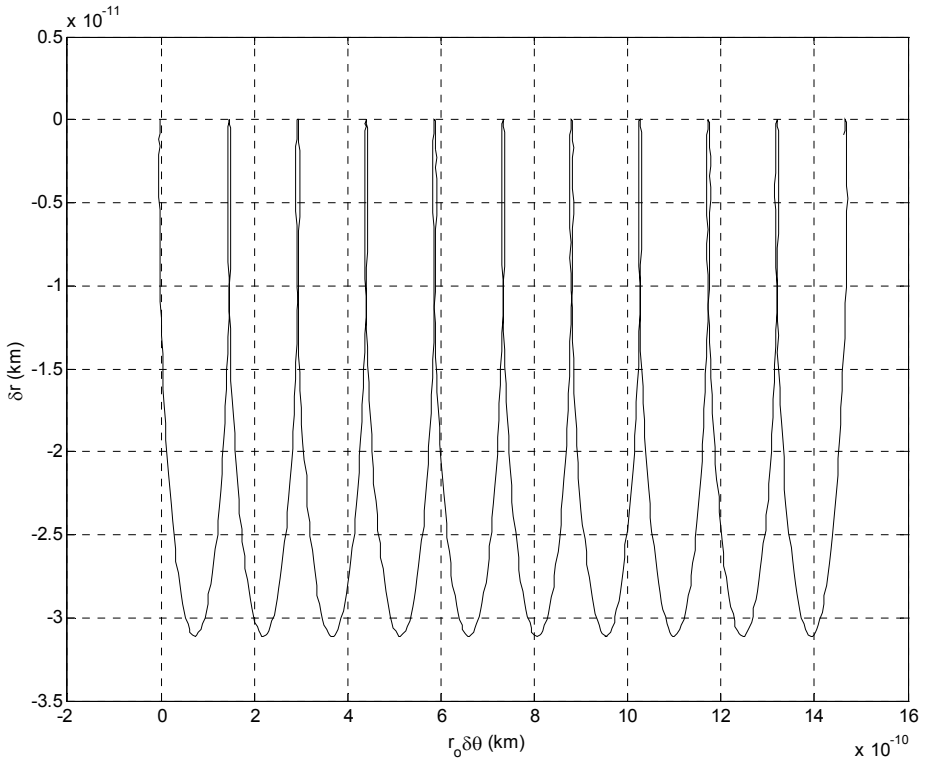

Figure 8 Simulator Error - Distance Between Linear and Non-Linear Propagations

Linear Versus Non-Linear Equations of Motion

As discussed in previous chapters, control inputs for this study are calculated using methods based on linear equations of motion. The orbits are then propagated using non-linear equations of motion. Before discussing the results of this project, it is enlightening to further explore the influence of linearization.

For the linearized equations to remain valid, only small δr and δz are allowed; however, $r_o \delta\theta$ may be large. Adding eccentricity to an orbit causes it to have a greater variation in δr compared to the circular reference orbit. For an orbit with the orbital elements listed in Table 2, there is a clear difference in the orbits propagated using the linear and non-linear equations of motion. The results are seen in Figure 9 which shows, in the δr, $r_o \delta\theta$ plane, the relative distance between the location of the satellite calculated using the linear equations of motion and the location of the satellite calculated using the non-linear equations of motion.

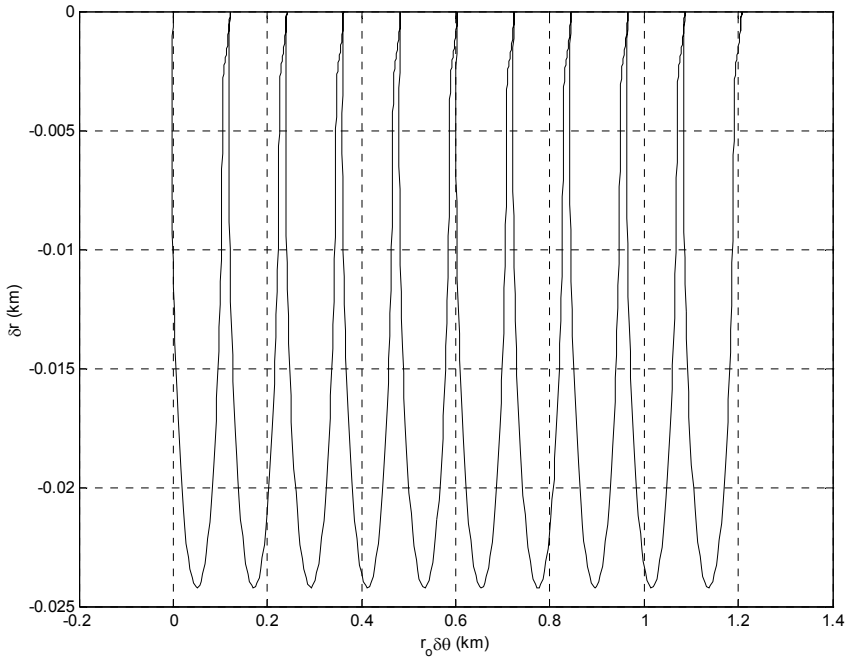

Figure 9 Distance Between Linear and Non-Linear Propagations With Eccentricity

It can be seen that there is a periodic difference in the radial direction during each orbit and a secular difference in the in-track direction. The peak δr offset in each orbit is approximately 24 meters and the $r_o \delta\theta$ accumulation is about 120 meters per orbit.

Repeating these calculations with the eccentricity changed to 0.00313260666343051 produces a graph of similar shape, but the magnitudes of the δr and $r_o \delta\theta$ offsets are approximately 240 meters and 1.2 kilometers per orbit, respectively. This corresponds to the orbit of the microsatellite after applying the delta-V calculated using the Clohessey-Wiltshire equation. Clohessey-Wiltshire results will be discussed in greater detail later.

To further illustrate the differences between the linear and non-linear equations of motion, Figure 10 shows the difference between the two as measured in an inertial frame

and Figure 11 shows the same difference as measured in the relative frame. Both figures represent the difference for the orbit defined in Table 2 and have been propagated over ten orbits.

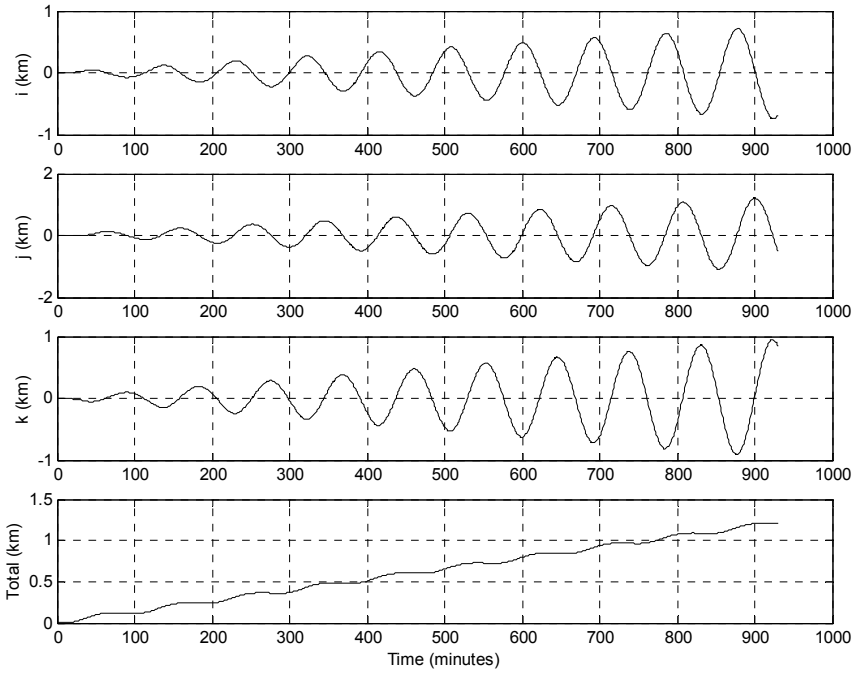

Figure 10 Difference in Linear and Non-Linear Propagation in Inertial Frame

The secular effect in the $r_o \delta\theta$ direction is clearly seen in the second graph of Figure 11.

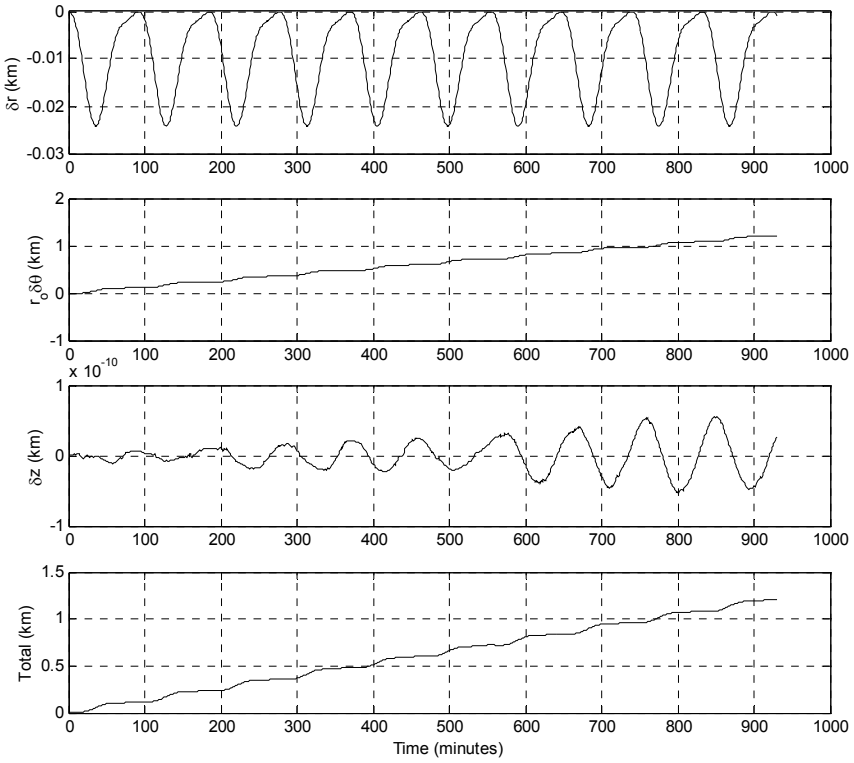

Figure 11 Difference in Linear and Non-Linear Propagation in Relative Frame

Clohessey-Wiltshire Controller

The Clohessey-Wiltshire equations have peculiar behavior, and careful selection of the desired rendezvous time is important for their performance. The top graph in Figure 12 was generated by varying the rendezvous time up to 6 six orbits. The reference orbit's semi-major axis length was used to calculate the necessary mean motion, n, the starting relative position was set at $\delta\bar{r} = \begin{bmatrix} 0 & -1000 & 0 \end{bmatrix}$, and the necessary relative velocity, $\delta\bar{v}$,

for a rendezvous at the origin, $\delta\vec{r} = \begin{bmatrix} 0 & 0 & 0 \end{bmatrix}$, was calculated. The magnitude of the calculated velocity, $|\delta\vec{v}|$, is shown.

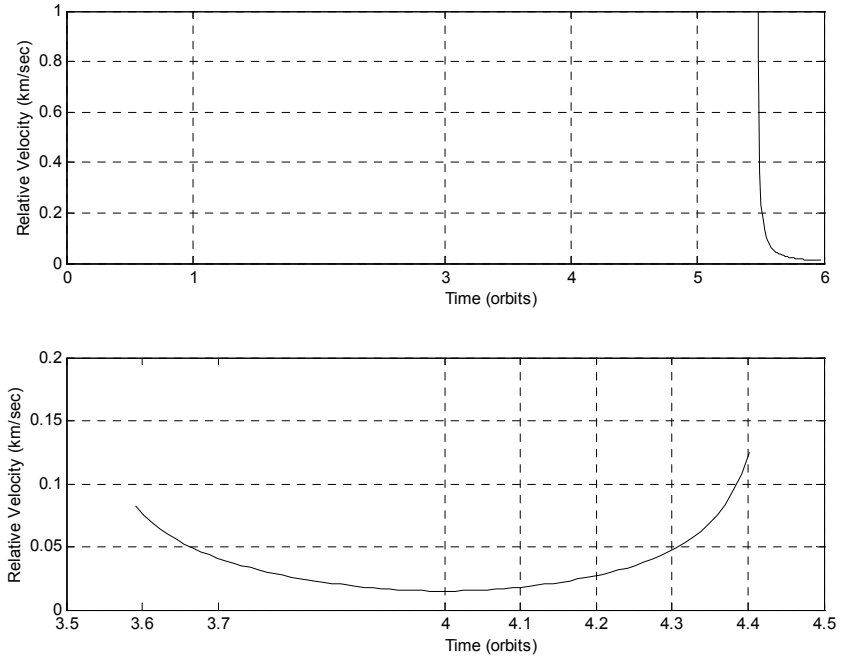

Figure 12 Magnitude of the Relative Velocity for Rendezvous to the Origin

The graph reveals that some selections of rendezvous time are very costly. Between each of the extreme occurrences are a range of more reasonable values. The lower graph in Figure 12 shows a closer view of the curve in the range of rendezvous times from 3.6 orbits to 4.4 orbits. Similar troughs are seen between the other extreme values. As the selected rendezvous time increases, the troughs reach lower $|\delta\vec{v}|$ values. It appears that for rendezvous to the origin, the best selection of rendezvous times are integer numbers of orbits.

Since the target in this study has non-zero eccentricity, it is unlikely to be at the reference orbit's origin at rendezvous time. To represent the potential offset from the origin, the runs from Figure 12 were repeated, but the target rendezvous position was set to $\delta\vec{r} = [10 \quad 10 \quad 0]$. The results are depicted in Figure 13. The closer view in the lower graph reveals the effect of an offset target is to add additional peak values in the troughs. These new peaks appear at integer numbers of orbits. Therefore, the best rendezvous times for this case are within each trough, close to an integer number of orbits but not an exact integer number of orbits.

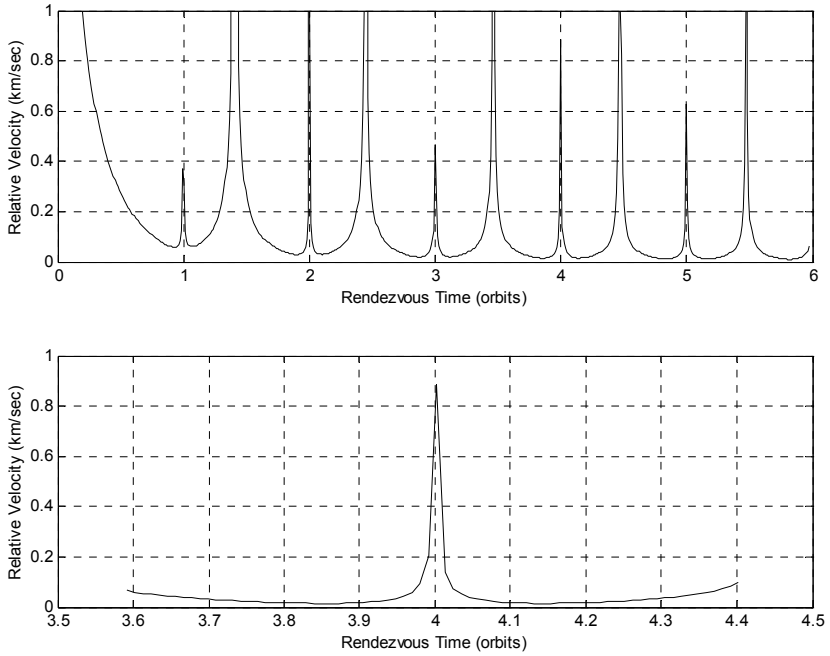

Figure 13 Magnitude of the Relative Velocity for Rendezvous to an Offset Location

Figure 14 shows the ΔV curve from 330 minutes to 400 minutes, for the rendezvous scenario considered in this chapter. Since the target satellite's orbital period is 92.45

minutes, exactly four orbits would take 369.8 minutes. A rendezvous time of 368 minutes, which is slightly less than four orbits, has been selected. This rendezvous time requires less ΔV than is found in troughs associated with a lower number of orbits, and within the trough depicted in Figure 14, it corresponds to the minimum ΔV immediately before the spike. Using a rendezvous time from a trough associated with a higher number of orbits would reduce the required ΔV, but the impact of propagating a linear solution using the non-linear equations of motion is secular, resulting in a larger final distance when a longer rendezvous time is used.

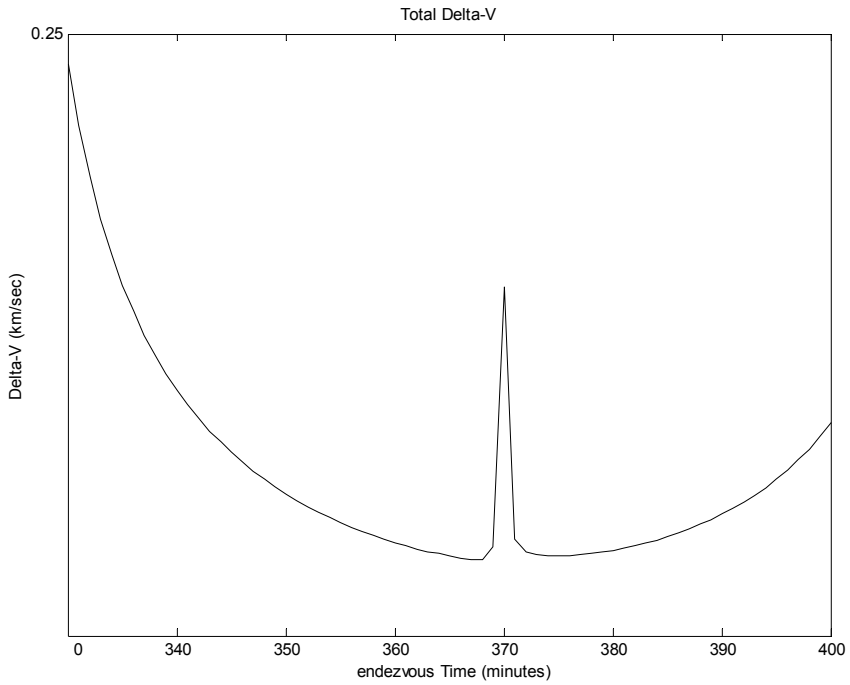

Figure 14 Delta-V Required to Achieve Rendezvous for the Considered Scenario

Using the specified rendezvous time of 368 minutes and including no perturbations, produces the results in Table 3. The initial ΔV is required to begin the rendezvous

maneuver and the second ΔV is performed at the rendezvous time to null out the relative velocity between the microsatellite and the target satellite. Since rendezvous to the target satellite has not been completely accomplished, further maneuvers will be necessary. Therefore, matching the target's velocity exactly is not actually desirable, but it is accomplished here to complete the results from a single rendezvous maneuver. Subsequent maneuvers to close the final distance using the Clohessey-Wiltshire controller were ineffective at completing the rendezvous to an acceptable distance, particularly if there was a significant δr offset. This can be readily seen in the examples illustrated in Tables 15 – 17 in Appendix A.

CW Rendezvous – No Perturbations	
ΔV_1 (km/sec)	0.016539
ΔV_2 (km/sec)	0.015269
ΔV_{Total} (km/sec)	0.031809
Final Distance (km) at 368 Minutes	5.029880

Table 3 CW Rendezvous – No Perturbations

Figure 15 shows how the relative distance between the microsatellite and target satellite decreases over time. The distances in the figure were calculated in the relative reference frame and propagated with the linear equations of motion.

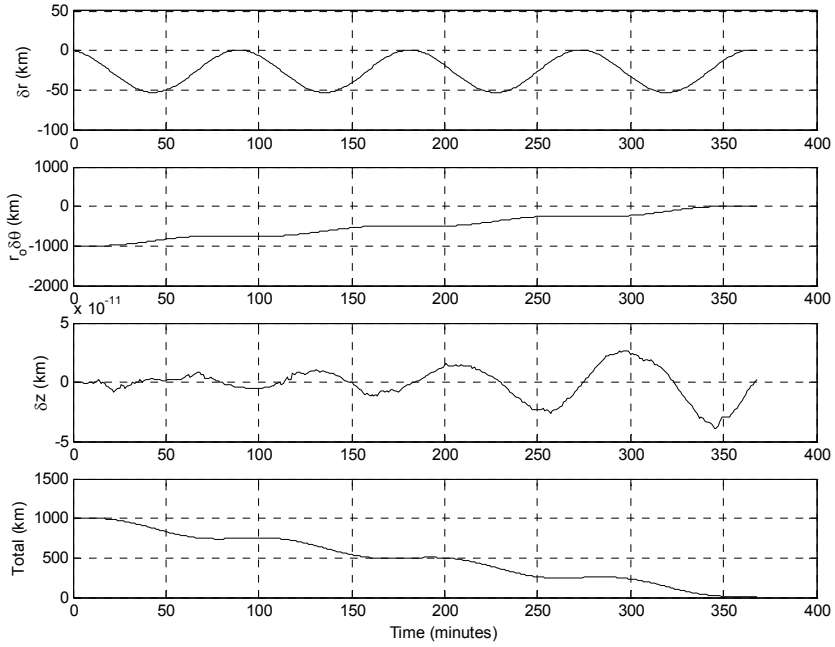

Figure 15 Relative Distance Between the Target and Microsatellite in Relative Frame

The same Delta-V solution was applied and propagated in the inertial reference frame using the non-linear equations, and the results of both propagations are depicted in Figure 16 along with the difference between the two. Both graphs have similar shape, but the difference between them is seen to be both periodic and secular with offsets as large as 23 kilometers during the maneuver.

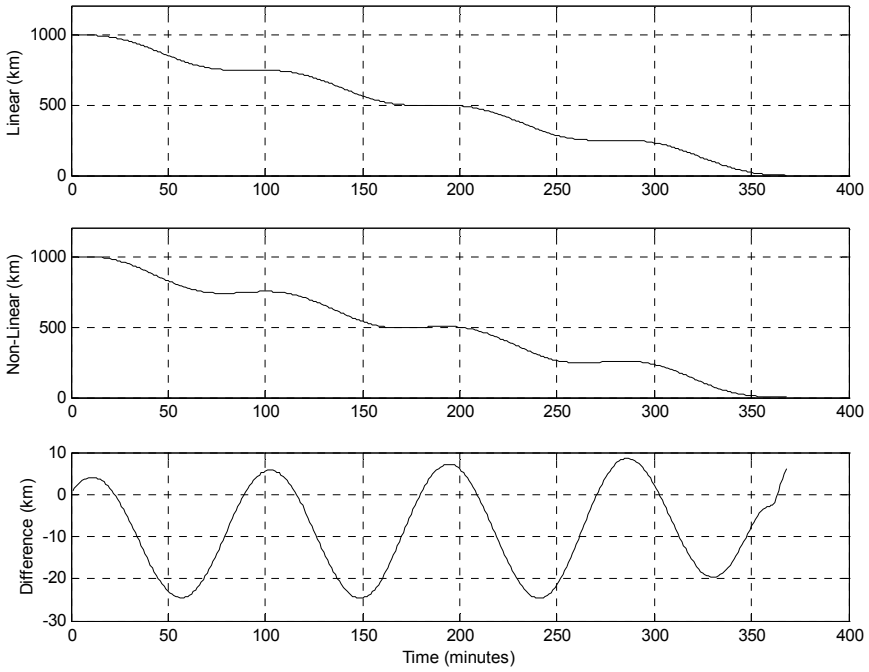

Figure 16 Linear and Non-Linear Propagation of Cloehessey-Wiltshire Solution

In Figure 17, the final rendezvous behavior is more closely examined. It can be seen that the linear propagator goes to a relative distance of zero precisely at 368 minutes, as expected. However, propagation using the non-linear equations has the effect of offsetting the time of closest approach, to a distance of 0.793406 kilometers at 362 minutes. At the specified rendezvous time of 368 minutes, the microsatellite is 5.029880 kilometers from the target satellite and is already moving away. This figure further illustrates the effect of using linear control equations to calculate maneuvers which are then applied using non-linear equations.

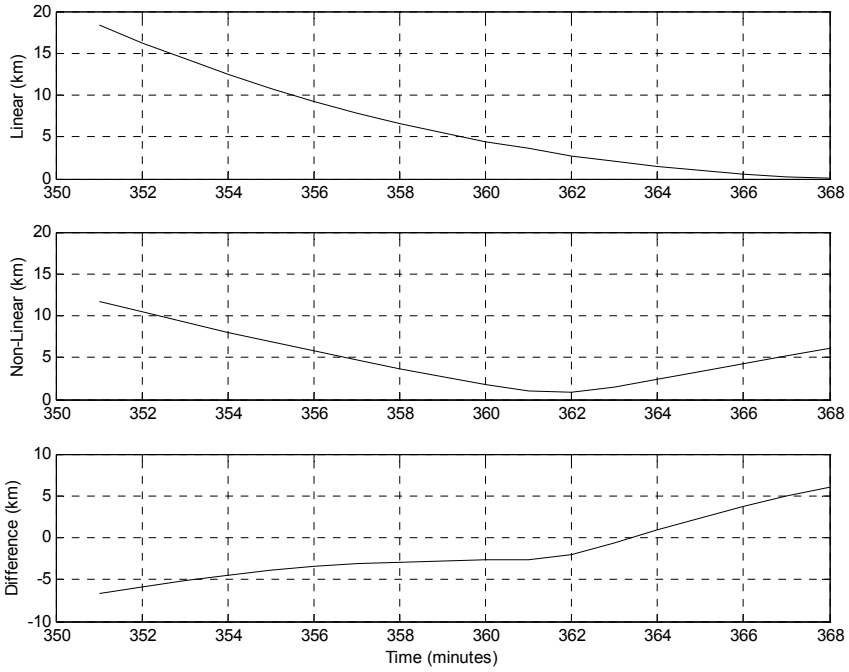

Figure 17 Closer View of Final Rendezvous Behavior

Adding the J_2 perturbation to both the propagator and the Clohessey-Wiltshire equations produces the results in Table 4. This rendezvous is depicted in Figure 18, which is rendered in the relative coordinate frame. Since the target has a non-zero inclination, the J_2 perturbation causes out of plane effects during the rendezvous which can be seen as divergence in the δz plot.

CW Rendezvous – J_2 Perturbation	
ΔV_1 (km/sec)	0.016578
ΔV_2 (km/sec)	0.015917
ΔV_{Total} (km/sec)	0.032496
Final Distance (km) at 368 Minutes	3.518942

Table 4 Clohessey-Wiltshire Rendezvous With J_2 Perturbation

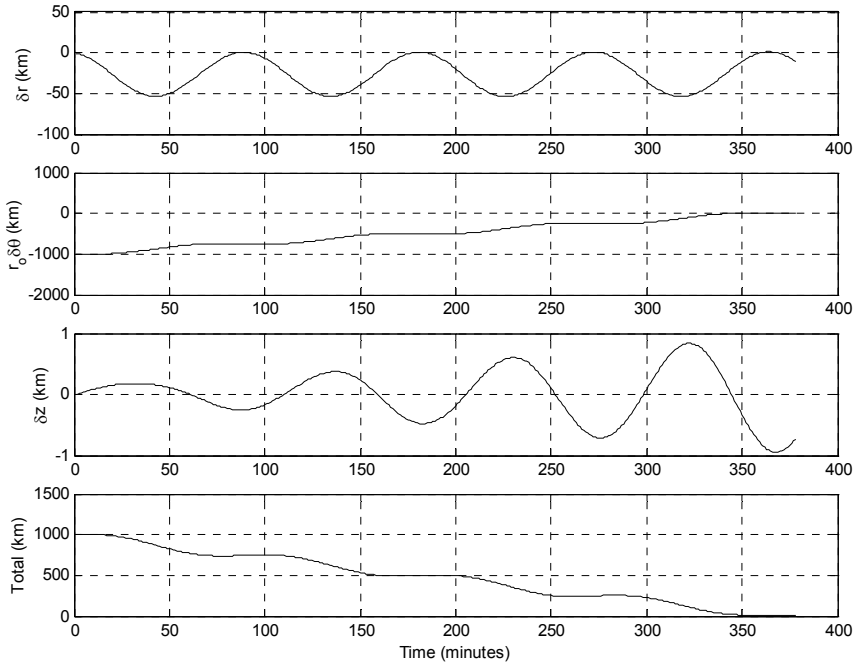

Figure 18 Clohessey-Wiltshire Rendezvous with J_2 Perturbation

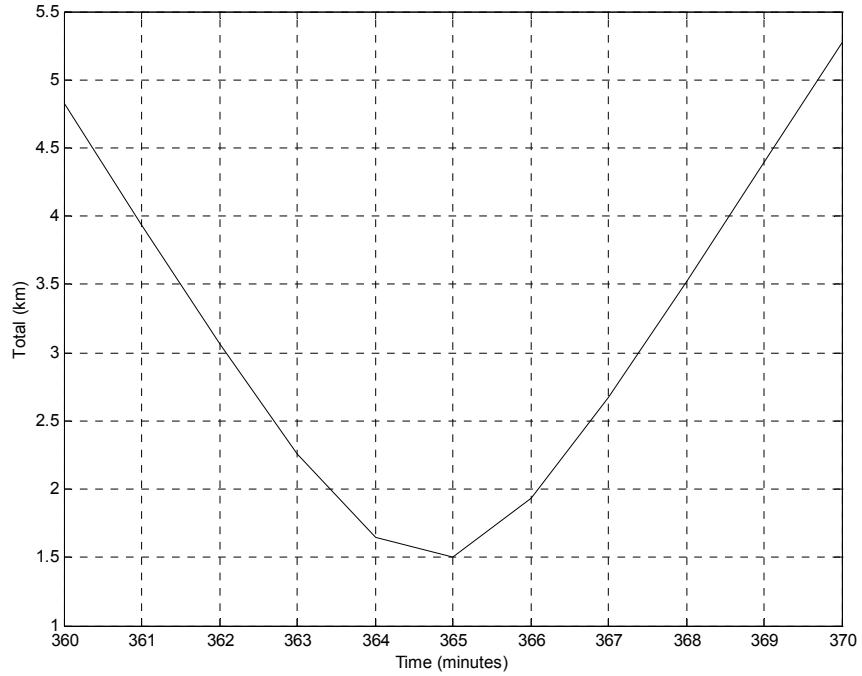

Figure 19 Closer View of Clohessey-Wiltshire Rendezvous with J_2 perturbation

Finally, the drag perturbation is added to the propagator. This produces the results listed in Table 5.

CW Rendezvous – J_2 and Drag Perturbations	
ΔV_1 (km/sec)	0.016578
ΔV_2 (km/sec)	0.019170
ΔV_{Total} (km/sec)	0.035748
Final Distance (km) at 368 Minutes	3.321252

Table 5 Clohessey-Wiltshire Rendezvous With J_2 and Drag Perturbations

The position of the microsatellite relative to the target satellite is depicted in Figure 20, for the Clohessey-Wiltshire solution with J_2 and drag perturbations included.

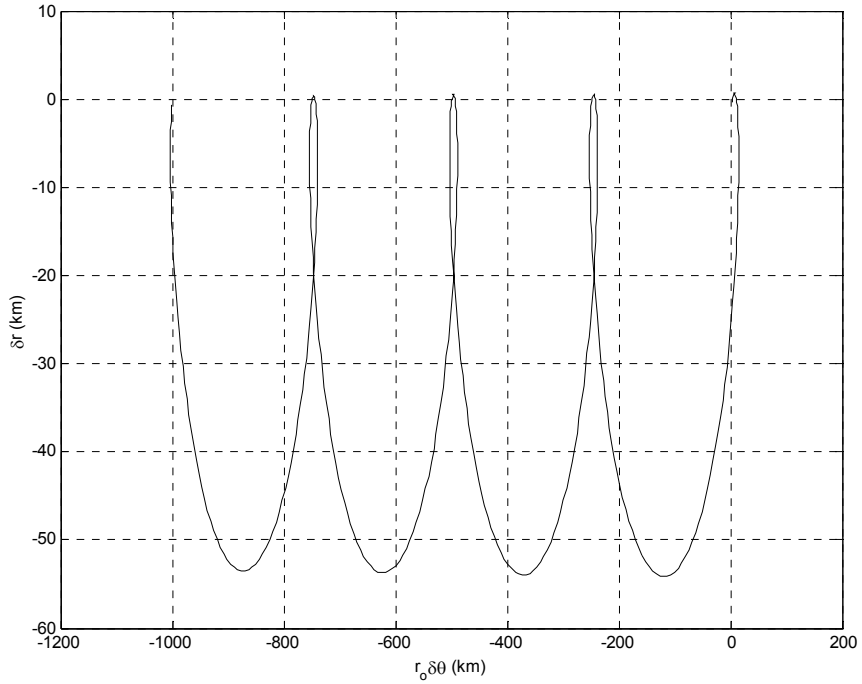

Figure 20 Clohessey-Wiltshire Rendezvous with Perturbations in Relative Frame

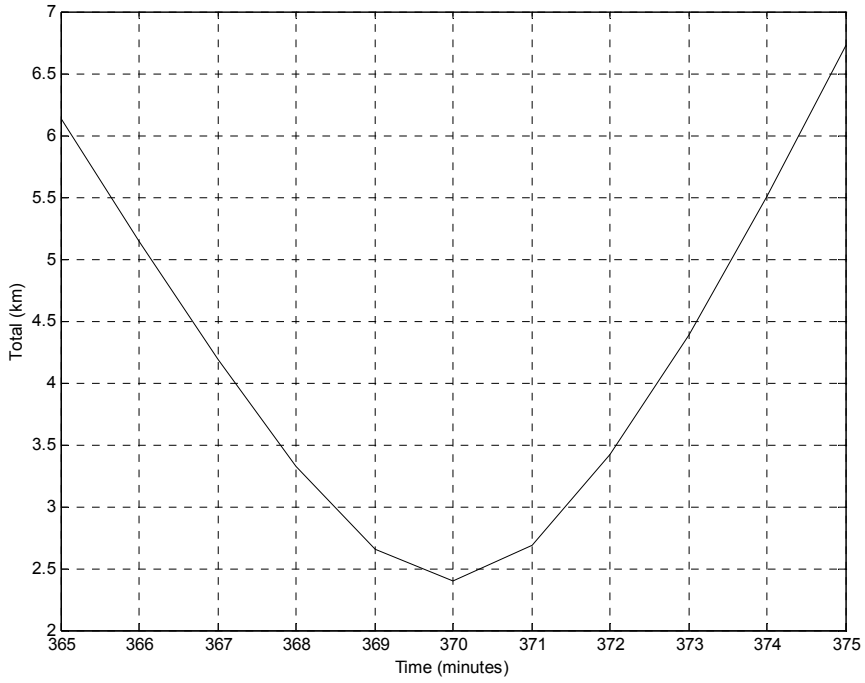

Figure 21 Closer View of Clohessey-Wiltshire Rendezvous with J_2 and Drag

A review of the distances for the Clohessey-Wiltshire cases discussed above reveals that the microsatellite is closer to the target satellite at the specified rendezvous time when the J_2 perturbation is added and even closer when drag is added. A closer study of the results reveals that rendezvous time is shifted from the specified time in each of these cases, and the closest approach does occur in the case when no perturbations are present. Adding perturbations causes the closest approach distance to increase.

Figure 22 shows that using the linear equations in the case when no perturbations are present results in rendezvous to zero distance at the specified time. Propagating the same solution using the non-linear equations causes the rendezvous to occur 6 minutes early, at 362 minutes. Adding the J_2 perturbation then delays the rendezvous by 3 minutes from

the non-perturbed case, to 365 minutes. Addition of drag further delays the rendezvous to 370 minutes.

CW Rendezvous Distances			
Case	Distance at 368 Minutes (km)	Time of Closest Approach (min)	Distance of Closest Approach (km)
No Perturbations	5.029880	362	0.793406
J_2 Perturbation	3.518942	365	1.499542
J_2 and Drag Perturbations	3.321252	370	2.398979

Table 6 Clohessey-Wiltshire Rendezvous Distances

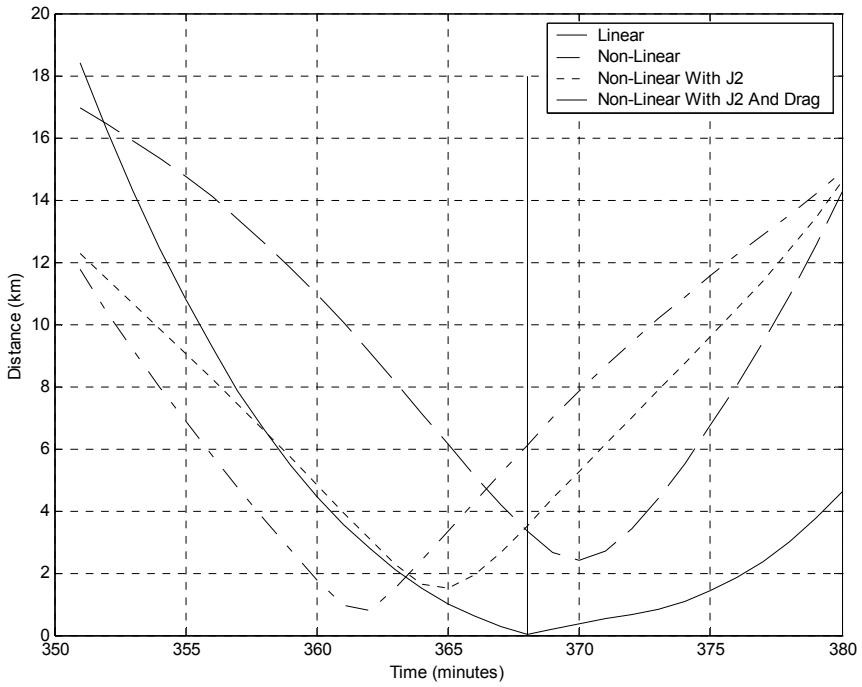

Figure 22 Clohessey-Wiltshire Rendezvous Results

Linear Quadratic Regulator Controller

With the Clohessey-Wiltshire controller, ΔV was influenced by adjusting the rendezvous time. With the Linear Quadratic Regulator (LQR) controller, ΔV is influenced by adjusting the values in the state weighting and control weighting matrices. Decreasing control usage generally saves fuel, but rendezvous may be delayed or not achieved.

Since rendezvous time is not fixed for this method, the controller is allowed to operate until the criteria that define a successful rendezvous are satisfied. For this project, two criteria were selected that must be concurrently satisfied for a successful rendezvous:

1. Achieve a relative distance of 1 meter or less
2. Achieve a relative velocity of 1 cm/sec or less.

For the case with no perturbations, the results are captured in Table 7. The state weighting matrix values are set to 1 and the control weighting matrix values are set to 1e13 for this case.

LQR Rendezvous – No Perturbations	
ΔV_{Total} (km/sec)	0.306821
Rendezvous Time (min)	510

Table 7 Linear Quadratic Regulator Rendezvous With No Perturbations

The relative distance between the microsatellite and the target satellite during the rendezvous is shown in Figure 23. The figure shows that the majority of the distance is reduced early in the pursuit, and most of the time is spent eliminating a relatively small final distance.

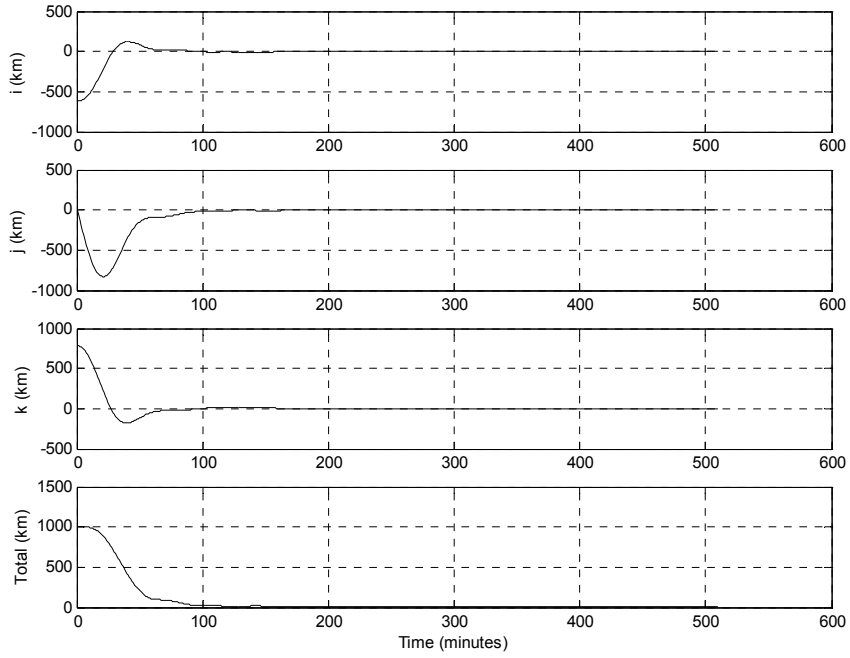

Figure 23 Relative Distance During LQR Rendezvous With No Perturbations

To compare similar rendezvous maneuvers using both of the controller methodologies and no perturbations, the rendezvous distance and velocity criteria for a Linear Quadratic Regulator rendezvous were temporarily set to 5.02988 km and 0.015269 km/sec, respectively, to correspond with the final values for a Clohessey-Wiltshire rendezvous at 368 minutes. The values in the control weighting matrix were then adjusted to achieve the Linear Quadratic Regulator rendezvous as close to 368 minutes as possible. This

proved difficult because of the sensitivity of the controller. Slightly lower control weighting resulted in the microsatellite circling the target satellite more times as it converged, while slightly higher control weighting produced a more direct flight route. However, the difference in ΔV between the more and less direct flight paths was minimal, less than 5 percent. The result achieved closest to 368 minutes was 321 minutes for rendezvous, which required 0.098694 km/sec of ΔV compared to 0.016539 km/sec for the initial ΔV in a similar Clohessey-Wiltshire rendezvous.

The Linear Quadratic Regulator rendezvous criteria were returned to a relative distance of 1 meter or less and a relative velocity of 1 cm/sec or less, and the J_2 perturbation was added producing the results in Table 8. The values for the state weighting matrix and the control weighting matrix were 1 and 1e13, respectively, and the rendezvous is depicted in Figure 24.

LQR Rendezvous – J_2 Perturbation	
ΔV_{Total} (km/sec)	0.308920
Rendezvous Time (min)	658

Table 8 LQR Rendezvous With J_2 Perturbation

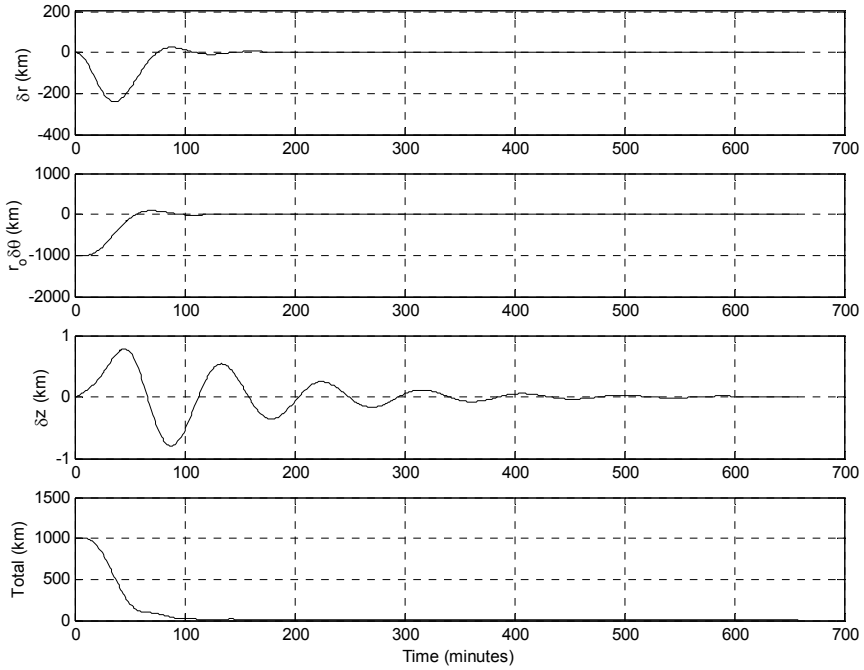

Figure 24 Relative Distance During LQR Rendezvous With J_2 Perturbation

The out of plane effect of the J_2 perturbation is seen to be the most time consuming for the controller to overcome. Countering the J_2 perturbation effect only increases the ΔV by 2.1 m/sec over the non-perturbed result. Therefore, the values corresponding to δz in the state weighting matrix are henceforth multiplied by 100 to speed transition to the final state. The new performance values are shown in Table 9 and the effect on rendezvous dynamics is pictured in Figure 25.

LQR Rendezvous – J_2 Perturbation	
ΔV_{Total} (km/sec)	0.308844
Rendezvous Time (min)	509

Table 9 LQR Rendezvous With J_2 Perturbation and Increased δz State Weighting

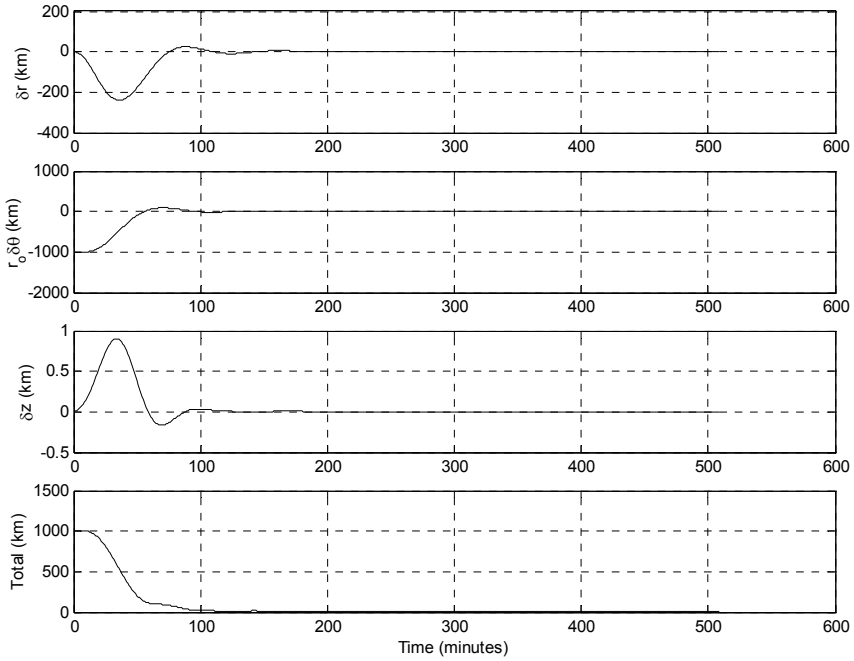

Figure 25 Relative Distance During LQR Rendezvous With J_2 Perturbation and Increased δz State Weighting

The increased weighting on the δz values in the state weighting matrix actually decreases the overall ΔV required for the maneuver slightly by decreasing the time for rendezvous 149 minutes.

Finally, the drag perturbation is added. The additional burden proves to be too great for the controller to overcome with the previous control weighting matrix values. Therefore, control emphasis was increased by lowering the values in the control weighting matrix by half, from 1e13 to 5e12. The increase in control emphasis is sufficient to achieve rendezvous, and results in a ΔV increase of more than 75 m/sec over the previous value, while the time to achieve rendezvous is reduced by nearly 2 hours. The performance values are found in Table 10 and the position of the microsatellite relative to the target satellite is captured in the δr, $r_o \delta\theta$ plane in Figure 26.

LQR Rendezvous – J_2 and Drag Perturbations	
ΔV_{Total} (km/sec)	0.383119
Rendezvous Time (min)	384

Table 10 LQR Rendezvous with J_2 and Drag Perturbations

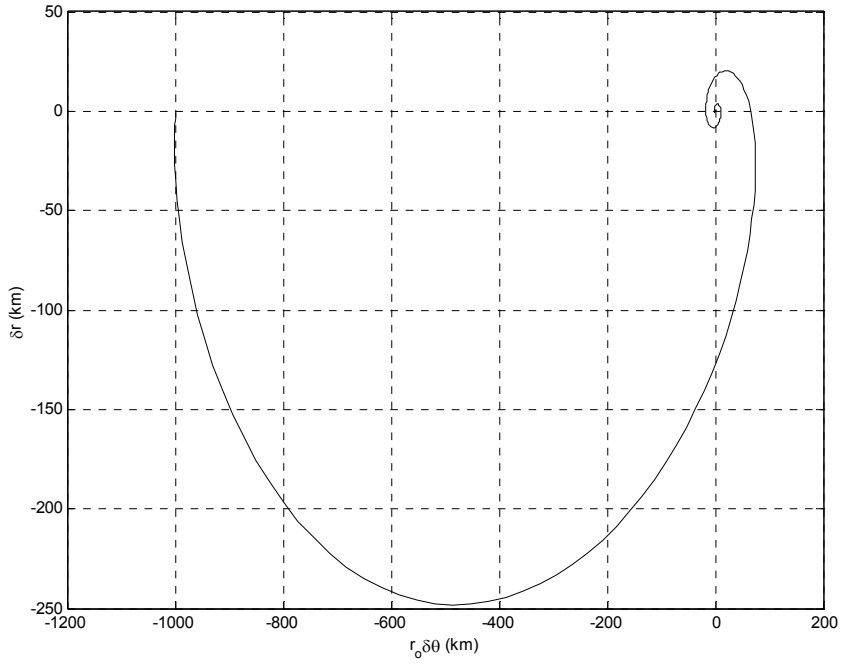

Figure 26 LQR Rendezvous with J_2 and Drag Perturbations in $\delta r, r_o \delta\theta$ plane

Hybrid Controller

The final controller considered is a hybrid controller. The Clohessey-Wiltshire controller has been shown to be useful for reducing large distances with low fuel usage, but it lacks sufficient robustness to complete the maneuver. The Linear Quadratic Regulator controller has been shown to be quite robust, but it uses a great deal of fuel in

reducing large distances. The logical solution is to combine the two controllers to exploit their strengths and minimizes their weaknesses.

The hybrid controller uses the Clohessey-Wiltshire controller to calculate the initial impulsive ΔV. Then the target is pursued until the specified rendezvous time. Instead of applying a second ΔV to null out the relative velocity, the position and velocity of the microsatellite relative to the target satellite at rendezvous time are fed directly into the Linear Quadratic Regulator controller as starting values. The LQR controller then completes the rendezvous to the specified relative position and velocity criteria. Since the LQR controller is only used to reduce a small distance at the end, the control emphasis can be increased without a significant penalty in ΔV. For the test cases in this section, the control weighting matrix values are set to 1e12.

As with the previous controllers, the first test case of the hybrid controller involves a rendezvous with no perturbations. The performance values are captured in Table 11 and the rendezvous is depicted in Figure 27.

Hybrid Rendezvous – No Perturbations	
ΔV_{CW} (km/sec)	0.016539
ΔV_{LQR} (km/sec)	0.026642
ΔV_{Total} (km/sec)	0.043181
Rendezvous Time (minutes)	574

Table 11 Hybrid Rendezvous With No Perturbations

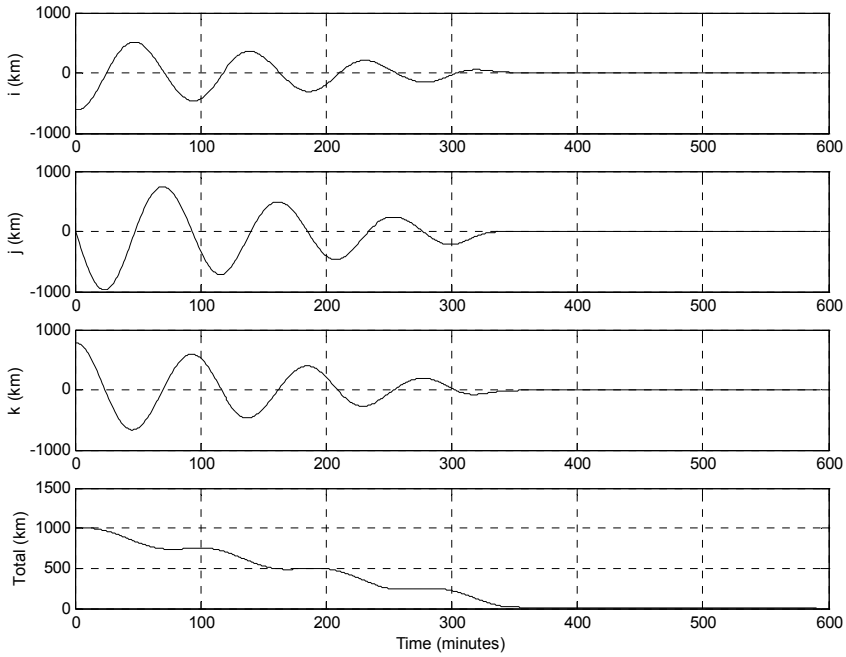

Figure 27 Hybrid Rendezvous With No Perturbations

Next, the J_2 perturbation is added to the scenario. The resultant performance values are listed in Table 12 and the maneuver is illustrated in Figure 28. Of particular interest is the δx graph which shows divergence during the Clohessey-Wiltshire portion of the rendezvous, then quickly gets damped out once the Linear Quadratic Regulator controller takes over.

Hybrid Rendezvous – J_2 Perturbation	
ΔV_{CW} (km/sec)	0.016578
ΔV_{LQR} (km/sec)	0.029722
ΔV_{Total} (km/sec)	0.046301
Rendezvous Time (minutes)	573

Table 12 Hybrid Rendezvous With J_2 Perturbation

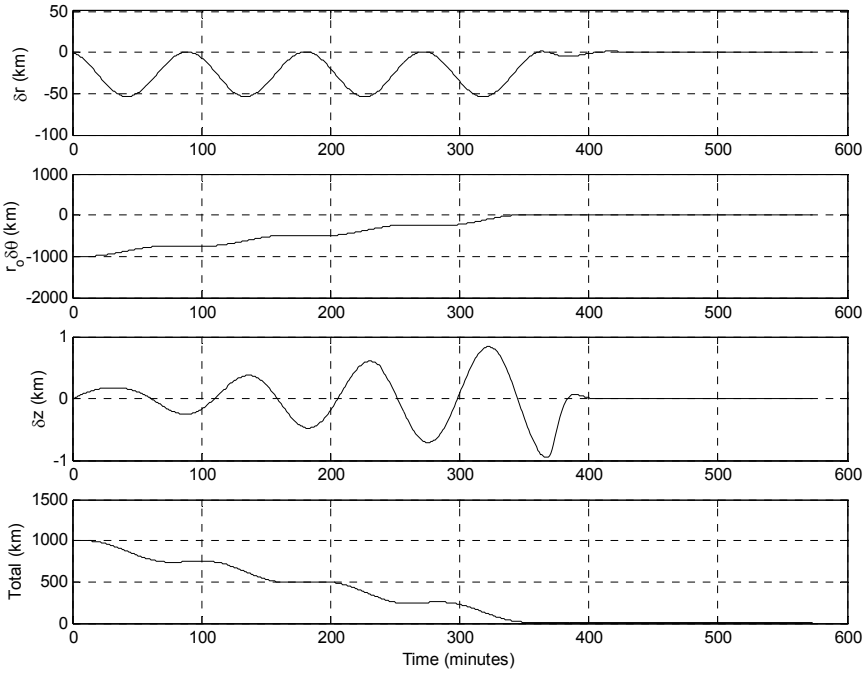

Figure 28 Hybrid Rendezvous With J_2 Perturbation

Drag is added for the final test case. The performance values are listed in Table 13 and the motion of the microsatellite relative to the target is plotted in Figure 29.

Hybrid Rendezvous – J_2 and Drag Perturbations	
ΔV_{CW} (km/sec)	0.016578
ΔV_{LQR} (km/sec)	0.032306
ΔV_{Total} (km/sec)	0.048885
Rendezvous Time (minutes)	590

Table 13 Hybrid Rendezvous With J_2 and Drag Perturbations

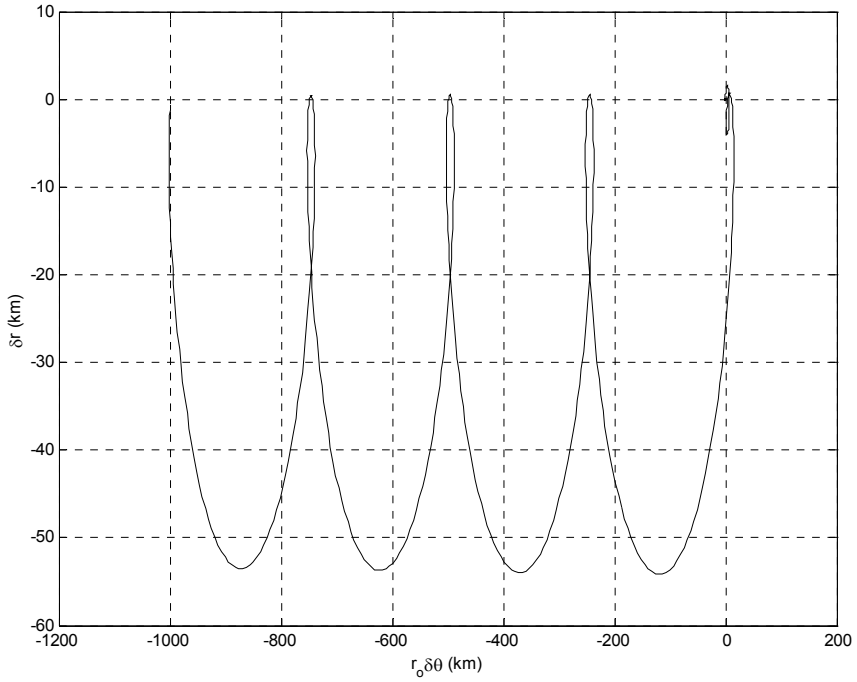

Figure 29 Hybrid Rendezvous with J_2 and Drag Perturbations in $\delta r, r_o \delta\theta$ plane

V. Conclusions and Recommendations

The important values from the test cases for all three controllers studied are compiled in Table 14.

Controller\Perturbations		No Perturbations	J_2 Perturbation	J_2 and Drag
CW	ΔV_{Total} (km/sec)	0.031809	0.032496	0.035748
	Distance (km)	5.029880	3.518942	3.321252
	Time (min)	368	368	368
LQR	ΔV_{Total} (km/sec)	0.306821	0.308844	0.383119
	Distance (km)	<0.001	<0.001	<0.001
	Time (min)	510	509	384
Hybrid	ΔV_{Total} (km/sec)	0.043181	0.046301	0.048885
	Distance (km)	<0.001	<0.001	<0.001
	Time (min)	574	573	590

Table 14 Compilation of Test Case Results For All Three Controllers

Conclusions

It can be readily seen that adding perturbation effects increases the needed ΔV for all three controllers. It is also clear that the Clohessey-Wiltshire controller uses the least ΔV, but does not achieve the desired rendezvous distance. Accomplishing multiple CW maneuvers is not effective either, especially if the δr offset is non-zero. This can be seen in Appendix A, where other examples of CW results over a range of δr and $r_o \delta\theta$ values can be found.

The Linear Quadratic Regulator controller achieves rendezvous to the desired relative distance and velocity, but spends a great deal of fuel in the process. Attempts to decrease fuel usage by adjusting the state weighting or control weighting matrices lengthen the amount of time required to achieve rendezvous, and if taken too far, could result in insufficient control usage to even complete the rendezvous.

The Hybrid controller is clearly the best solution. It achieves rendezvous to the specified relative distance and velocity while only increasing ΔV by approximately 50% over the corresponding values for the Clohessey-Wiltshire controller.

The results of this study suggest that the control portion of the microsatellite rendezvous is feasible with reasonable fuel usage.

Recommendations

In the test cases used for this study, the microsatellite began rendezvous from 1000 kilometers in-track ($r_o \delta\theta$) behind the target satellite. Further study should include varying the starting location in all three directions, in-track, radial (δr) and out of plane (δz). Some examples of varying starting position in the in-track and radial directions are found in Appendix A.

This study focused on satellites in Low Earth Orbit. Future study should expand to include higher orbits. Additionally, this study included a small eccentricity in the target orbit. Future investigation should include increasing the target orbit's eccentricity to explore the performance envelope of the controllers.

The Clohessey-Wiltshire equations need to be further developed to account for inclination differences between the microsatellite and the target satellite. Development of the differential inclination terms is discussed by Swank, et al. (8)

The greatest potential for improvement in controller performance is incorporation of gain scheduling in the Linear Quadratic Regulator. The control usage should begin low to avoid drastic maneuvers which can be costly in fuel, and then increase as the microsatellite approaches the target, to complete the rendezvous. To implement gain scheduling, the optimal gain matrix could be recalculated in each iteration of the propagation algorithm. The control weighting could be set proportional to the remaining distance between the microsatellite and the target satellite.

This study was conducted as though perfect knowledge of the microsatellite's and the target satellite's position and velocity were known at all times. Future study should incorporate realistic uncertainties in these values, and performance of the controllers should be characterized statistically. Incorporation of a sequential filter seems to be the logical next step.

Finally, a systems engineering study should be conducted to determine the feasibility of implementing the control solutions investigated in this thesis. The propulsion system, processor, and onboard sensor capability should be key areas of focus.

Appendix A Example Controller Results

This appendix contains tables showing controller solution results over a range of starting offsets. The in-track offset ($r_o \delta\theta$) is varied from -1000 kilometers to +1000 kilometers while the radial offset (δr) is varied from -1 kilometer to +1 kilometer. No offsets in the out of plane direction (δz) are included.

Tables 15 – 17 are the results of using the Clohessey-Wiltshire controller. Table 15 was generated without perturbations; Table 16 includes the J_2 perturbation and Table 17 adds the drag perturbation. All Clohessey-Wiltshire solutions calculated in these tables use a rendezvous time of 368 minutes, though it should be clear from previous discussion that the optimal rendezvous time will vary with the relative geometry of the microsatellite and target satellite to the circular reference frame. The top value in each cell is the total ΔV (km/sec) needed for the maneuver, and the lower is the relative distance (km) at the specified rendezvous time.

Tables 18 – 20 are the results of using the Linear Quadratic Regulator controller. Table 18 was generated without perturbations; Table 19 includes the J_2 perturbation and Table 20 adds the drag perturbation. All LQR solutions were calculated with state weighting matrix values of 1. Table 18 and Table 19 were calculated using control weighting matrix values of 1e13 while the control weighting matrix value used for Table 20 is 1e12. The top value in each cell represents the total ΔV (km/sec) for the maneuver. The lower number is the time that it takes in integer minutes for the

microsatellite to rendezvous to within the specified criteria for relative distance ($\leq$ 1m) and relative velocity ($\leq$ 1cm/sec) of the target satellite.

Tables 21 – 23 are the results of using the Hybrid controller. Table 21 was generated without perturbations; Table 22 includes the J_2 perturbation and Table 23 adds the drag perturbation. For all Hybrid controller solutions in these tables, the CW portion was calculated using a rendezvous time of 368 minutes, and the LQR solutions used state weighting matrix values of 1 and control weighting matrix values of 1e12. The top value in each cell represents the total ΔV (km/sec) for the maneuver. The lower number is the time that it takes in integer minutes for the microsatellite to rendezvous to within the specified criteria for relative distance ($\leq$ 1m) and relative velocity ($\leq$ 1cm/sec) of the target satellite.

	-1000	-100	-10	-1	0	1	10	100	1000
1	0.03445	0.01857	0.01946	0.01958	0.01960	0.01961	0.01974	0.02127	0.05084
	5.58052	0.84143	1.15968	1.19841	1.20280	1.20719	1.24745	1.71914	13.8511
0.1	0.03159	0.00318	0.00182	0.00191	0.00192	0.00193	0.00207	0.00451	0.03738
	5.05209	0.16314	0.06485	0.09129	0.09439	0.09752	0.12681	0.50169	11.7393
0	0.03180	0.00332	3.35E-4	3.35E-5		3.35E-5	3.35E-4	0.00337	0.03619
	5.02988	0.24071	0.03131	0.00320		0.00322	0.03293	0.40283	11.5476
-0.1	0.03212	0.00439	0.00206	0.00193	0.00191	0.00190	0.00181	0.00313	0.03507
	5.01508	0.31387	0.11700	0.09181	0.08902	0.08623	0.06210	0.31697	11.3650
-1	0.03873	0.02019	0.01896	0.01885	0.01884	0.01882	0.01872	0.01783	0.02956
	5.21682	0.74610	0.68924	0.68031	0.67930	0.67829	0.66904	0.59703	10.1483

Table 15 CW Solutions Without Perturbations

	-1000	-100	-10	-1	0	1	10	100	1000
1	0.03292	0.01764	0.01979	0.02005	0.02008	0.02011	0.02037	0.02339	0.07507
	4.27274	0.23973	1.03635	1.17372	1.18919	1.20469	1.34594	2.92660	35.1488
0.1	0.03202	0.00340	0.00171	0.00194	0.00197	0.00200	0.00227	0.00594	0.05954
	3.55563	1.21481	0.06536	0.07447	0.08863	0.10301	0.23663	1.74987	33.1284
0	0.03249	0.00420	4.33E-4	4.34E-5		4.35E-5	4.36E-4	0.00448	0.05802
	3.51894	1.29209	0.14557	0.01472		0.01475	0.14921	1.65601	32.9425
-0.1	0.03307	0.00560	0.00226	0.00199	0.00196	0.00193	0.00170	0.00357	0.05655
	3.49129	1.36253	0.22425	0.09607	0.08204	0.06822	0.07474	1.56994	32.7643
-1	0.04170	0.02206	0.01956	0.01931	0.01928	0.01925	0.01901	0.01663	0.04608
	3.65082	1.68858	0.65572	0.54851	0.53689	0.52536	0.42699	1.17010	31.5111

Table 16 CW Solutions With J_2 Perturbations

	-1000	-100	-10	-1	0	1	10	100	1000
1	0.03180	0.01396	0.01628	0.01655	0.01659	0.01662	0.01691	0.02017	0.07335
	2.69499	3.47650	2.11697	1.97274	1.95656	1.94036	1.79366	0.67160	33.5371
0.1	0.03490	0.00646	0.00357	0.00340	0.00339	0.00337	0.00324	0.00399	0.05787
	3.27023	4.50285	3.15144	3.00127	2.98441	2.96753	2.81408	1.14845	31.5088
0	0.03574	0.00757	0.00389	3.53E-3		3.49E-3	0.00343	0.00366	0.05635
	3.32125	4.58521	3.23852	3.08872		3.05507	2.90196	1.23276	31.3205
-0.1	0.03666	0.00911	0.00577	0.00549	0.00546	0.00543	0.00517	0.00418	0.05489
	3.36905	4.66120	3.31944	3.17007	3.15330	3.13650	2.98379	1.31361	31.1397
-1	0.04745	0.02585	0.02314	0.02288	0.02285	0.02282	0.02255	0.01993	0.04448
	3.65081	5.05811	3.76722	3.62303	3.60684	3.59062	3.44309	1.81961	29.8511

Table 17 CW Solutions With J_2 and Drag Perturbations

	-1000	-100	-10	-1	0	1	10	100	1000
1	0.30791	0.03211	0.00428	0.00156	0.00128	0.00102	0.00210	0.03029	0.33944
	510	425	347	286	282	280	310	424	506
0.1	0.30693	0.03110	0.00322	4.28E-4	1.28E-4	2.10E-4	0.00300	0.03129	0.34050
	510	425	318	241	199	228	317	424	506
0	0.30682	0.03099	0.00311	3.11E-4		3.11E-4	0.00312	0.03140	0.34062
	510	424	317	235		235	317	424	506
-0.1	0.30671	0.03088	0.00300	2.10E-4	1.28E-4	4.28E-4	0.00323	0.03152	0.34074
	510	424	317	228	199	241	318	424	506
-1	0.30572	0.02988	0.00210	0.00102	0.00128	0.00156	0.00428	0.03253	0.34180
	510	424	310	280	282	286	347	425	506

Table 18 LQR Solutions Without Perturbations

	-1000	-100	-10	-1	0	1	10	100	1000
1	0.30994	0.03199	0.00426	0.00156	0.00128	0.00102	0.00210	0.03015	0.33706
	509	424	346	285	282	280	309	422	505
0.1	0.30895	0.03099	0.00321	4.26E-4	1.28E-4	2.09E-4	0.00299	0.03115	0.33811
	509	423	317	240	199	227	316	423	505
0	0.30884	0.03088	0.00310	3.10E-4		3.10E-4	0.00310	0.03126	0.33823
	509	423	316	235		235	316	423	505
-0.1	0.30873	0.03077	0.00299	2.09E-4	1.28E-4	4.26E-4	0.00321	0.03137	0.33835
	509	423	316	227	199	240	317	423	505
-1	0.30775	0.02978	0.00209	0.00102	0.00128	0.00156	0.00426	0.03238	0.33940
	509	423	309	280	282	285	346	424	505

Table 19 LQR Solutions With J_2 Perturbation

	-1000	-100	-10	-1	0	1	10	100	1000
1	0.70570	0.07758	0.00945	0.00269	0.00202	0.00130	0.00595	0.07535	0.83859
	301	239	183	187	310	132	206	217	275
0.1	0.70416	0.07598	0.00782	9.43E-4	2.01E-4	6.06E-4	0.00749	0.07695	0.84026
	301	239	182	124	121	141	207	217	275
0	0.70399	0.07580	0.00764	7.64E-4		7.79E-4	0.00767	0.07713	0.84045
	301	239	181	122		144	207	217	275
-0.1	0.70382	0.07562	0.00746	5.95E-4	2.12E-4	9.60E-4	0.00784	0.07731	0.84064
	301	239	181	120	99	146	207	218	275
-1	0.70228	0.07403	0.00592	0.00133	0.00198	0.00269	0.00948	0.07892	0.84231
	301	239	179	155	154	155	208	218	275

Table 20 LQR Solutions With J_2 and Drag Perturbations

	-1000	-100	-10	-1	0	1	10	100	1000
1	0.03834	0.02072	0.02210	0.02227	0.02228	0.02230	0.02247	0.02442	0.05463
	577	563	564	564	564	564	564	564	567
0.1	0.04214	0.00364	0.00204	0.00219	0.00221	0.00223	0.00243	0.00555	0.04207
	574	520	506	507	507	507	507	529	549
0	0.04318	0.00415	4.12E-4	2.55E-5		2.55E-5	4.11E-4	0.00413	0.04097
	574	513	452	374		374	451	512	549
-0.1	0.04431	0.00558	0.00243	0.00223	0.00221	0.00219	0.00204	0.00361	0.03995
	574	531	507	507	507	507	506	519	549
-1	0.05785	0.02438	0.02220	0.02200	0.02198	0.02196	0.02177	0.02017	0.03552
	575	565	564	564	564	564	564	563	560

Table 21 Hybrid Solutions Without Perturbations

	-1000	-100	-10	-1	0	1	10	100	1000
1	0.03925	0.02071	0.02285	0.02310	0.02312	0.02315	0.02340	0.02621	0.07039
	575	563	564	564	564	564	564	565	579
0.1	0.04505	0.00388	0.00204	0.00226	0.00229	0.00232	0.00261	0.00657	0.05644
	573	457	506	507	507	508	509	531	561
0	0.04630	0.00485	4.85E-4	4.80E-5		4.80E-5	4.86E-4	0.00494	0.05513
	573	506	440	425		425	440	503	560
-0.1	0.04763	0.00649	0.00261	0.00232	0.00229	0.00226	0.00203	0.00396	0.05388
	573	532	509	508	507	507	506	497	559
-1	0.06262	0.02605	0.02310	0.02283	0.02280	0.02277	0.02250	0.02007	0.04596
	586	565	564	564	564	564	564	563	553

Table 22 Hybrid Solutions With J_2 Perturbation

	-1000	-100	-10	-1	0	1	10	100	1000
1	0.03920	0.01904	0.02125	0.02150	0.02153	0.02156	0.02182	0.02465	0.06925
	549	562	562	562	562	562	562	563	561
0.1	0.04747	0.00611	0.00289	0.00276	0.00275	0.00274	0.00270	0.00549	0.05531
	591	520	517	516	516	516	516	514	556
0	0.04888	0.00725	0.00309	2.71E-3		2.66E-3	0.00260	0.00432	0.05400
	590	524	521	520		520	520	517	556
-0.1	0.05036	0.00892	0.00504	0.00472	0.00469	0.00466	0.00438	0.00416	0.05276
	590	527	525	524	524	524	524	521	555
-1	0.06608	0.02817	0.02499	0.02469	0.02466	0.02462	0.02433	0.02170	0.04489
	590	585	584	584	584	584	584	584	546

Table 23 Hybrid Solutions With J_2 and Drag Perturbations

Appendix B Linear Quadratic Regulator Propagation Algorithm

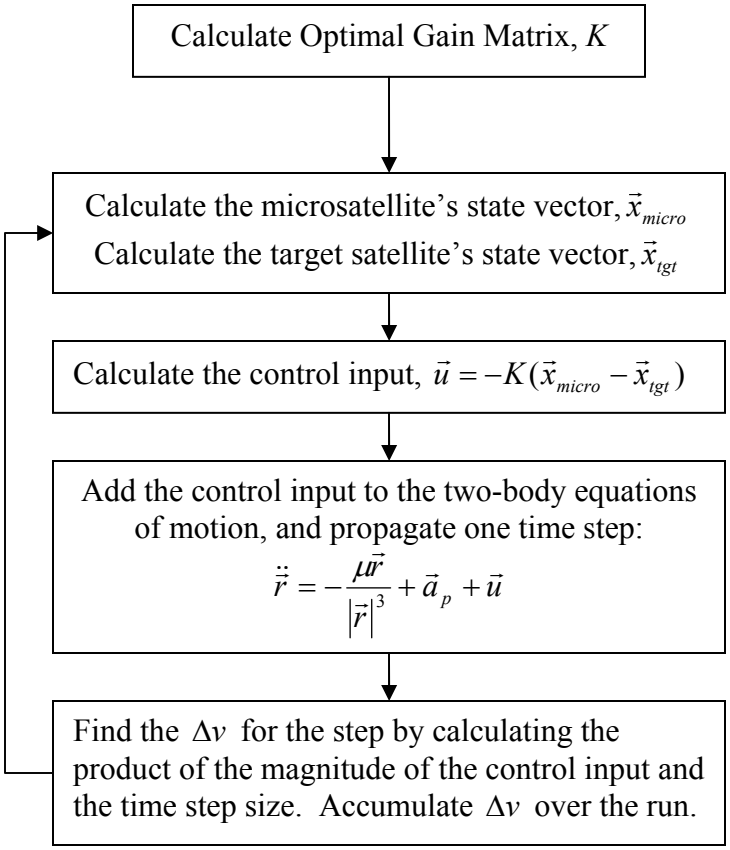

Appendix C MATLAB Code

MAIN

```
%================================================================
%
%  THESIS - MAIN CODE
%
%  AS OF:  04 MAR 03
%
%  Troy Tschirhart
%
%  Orbital Rendezvous With a Non-Cooperative Target
%
%----------------------------------------------------------------------------------------------------
%
%  This program uses the following function files which must be on the current path:
%
%  atmosphere.m    calculate atmospheric density at the given altitude
%  CalcInit.m      calculate the initial conditions for the run
%  CW_Rend         accomplish clohessey-wiltshire rendezvous maneuver
%  cw_v_ijk        calculate the clohessey-wiltshire velocity in inertial frame
%  Do_Plots        plot the results
%  LQR_Rend        accomplish lqr rendezvous manuever
%  propagate.m     propagator
%  posvel.m        set up the differential equation for the propagator
%  ijk2pqw.m       transform r,v from ijk frame to pqw frame
%  pqw2ijk.m       transform r,v from pqw frame to ijk frame
%  rtz2pqw.m       transform r,v from rtz frame to pqw frame
%  rv2coe.m        calculate coe for the given r,v
%  coe2rv.m        calculate r,v for the given coe
%
%================================================================
```

```
%=========================================================================
%
%  Clear Variables and Set Format Options
%
%=========================================================================

clear
format long g
format compact


%=========================================================================
%
%  Print a banner to separate results
%  Start the timer (used at the end to determine how long the run took)
%
%=========================================================================

('=========================================================================')

tic

%=========================================================================
%
%  Set Selectable Variable Values
%
%=========================================================================


%-------------------------------------------------------------------------------------------------------
%  The target's actual initial COEs
%-------------------------------------------------------------------------------------------------------

coe_tgt_act(1) = 6.772888912204840e+003;   %  km              a
coe_tgt_act(2) = 9.887713549825913e-004;   %  dimensionless   e
coe_tgt_act(3) = 0.79736386485827;         %  radians         nu
coe_tgt_act(4) = 0.90757990078380;         %  radians         i
coe_tgt_act(5) = 1.51843760980691;         %  radians         cap_omega
coe_tgt_act(6) = 5.59054044657763;         %  radians         small_omega
coe_tgt_act(7) = 0.0;                      %  seconds         time since perigee
```

```
%-------------------------------------------------------------------------------------------------------
%  Set initial micro offset from the target
%-------------------------------------------------------------------------------------------------------

dist = -1000;                    % kilometers arclength (ro*delta_theta)

delr = 0;                        % kilometers (delta_r)

delz = 0;                        % kilometers (delta_z)


%-------------------------------------------------------------------------------------------------------
%  Set the acceptable relative distance and velocity for a successful rendezvous
%-------------------------------------------------------------------------------------------------------

catchdis = 0.001;      % kilometers

catchvel = 0.00001;  % kilometers/second


%-------------------------------------------------------------------------------------------------------
%  Set controller options (Notes: "1" = option selected; "0" = option not selected;
%                    Only one controller option below should be selected for each run)
%-------------------------------------------------------------------------------------------------------

CW = 1;         % Use the Clohessey-Wiltshire controller only

CWLR = 0;     % Use the Clohessey-Wiltshire - LQR hybrid controller

LR = 0;         % Use the LQR controller only



%-------------------------------------------------------------------------------------------------------
%  Set step size and CW rendezvous time
%-------------------------------------------------------------------------------------------------------

timestep = 60;              % seconds

rend_time = 368;            % Integer number of timesteps
                            % Examples: For a rendezvous time of 184 minutes
                            % 184 if timestep = 60; 11040 [=184*60] if timestep = 1
```

```
%-------------------------------------------------------------------------------------------------------
%  Specify values for the state weighting matrix, Q
%  and the control weighting matrix, R
%  Note:  Q_mag increases => faster movement from initial to desired states
%         R_mag increases => lower control usage
%-------------------------------------------------------------------------------------------------------

Q_mag = 1;
R_mag = 1e13;


%-------------------------------------------------------------------------------------------------------
%  Set perturbation (J2) option (Note: "1" = option selected; "0" = option not selected)
%-------------------------------------------------------------------------------------------------------

pert = 0;                                          % Include perturbation terms


%-------------------------------------------------------------------------------------------------------
%  Set drag options and values (Note: "1" = option selected; "0" = option not selected)
%-------------------------------------------------------------------------------------------------------

dragtgt = 0;                                       % Include drag in target's propagations

cd_tgt = 2.2;                                      % Drag coefficient of the target

a_tgt = 3.5*1.2/(1000^2);                          % Area of the target (km^2)

m_tgt = 725;                                       % Mass of the target

cdamtgt = dragtgt * (cd_tgt * a_tgt) / m_tgt;      % Calculate the target's cdam value

%-------------------------------------------------------------------------------------------------------

dragmic = 0;                                        % Include drag in micro's propagations

cd_mic = 3;                                         % Drag coefficient of the micro

a_mic = 1.5/(1000^2);                               % Area of the micro (km^2)

m_mic = 100;                                        % Mass of the micro

cdammic = dragmic * (cd_mic * a_mic) / m_mic;       % Calculate the micro's cdam value
```

```
%-------------------------------------------------------------------------------------------------
%  Set plot options (Note: "1" = option selected; "0" = option not selected)
%-------------------------------------------------------------------------------------------------

prdijk = 1;     % Plot relative distance in the inertial (ijk) frame

prdrtz = 1;     % Plot relative distance in the relative (rtz) frame

prdroto = 1;    % Plot relative distance in the relative plane (delta_r, ro*delta_theta)


%=================================================================
%
%  Initialize variable values
%
%=================================================================

points = rend_time + 1;    % set the number of points for propagation
                            % (note: point 1 is really 0)

delta_v_accum = 0;         % initialize delta-V to zero



%=================================================================
%
%  Calculate Initial Values
%
%  1.  Target's initial position and velocity
%  2.  Micro's initial position and velocity
%
%=================================================================

CalcInit
```

```
%=========================================================================
%
%  Accomplish Clohessy-Wiltshire Rendezvous
%
%  1.  Determine the micro's position relative to the circular reference at the start time
%  2.  Determine the target's position relative to the circular reference at CW rend time
%  3.  Solve the CW equations
%  4.  Transform the delta-V from the relative frame to the inertial frame
%  5.  Apply the delta-V to the micro
%  6.  Fly out the micro and the target to rendezvous time
%  7.  Check final relative distance and velocity between the micro and the target
%
%=========================================================================

if (CW == 1) | (CWLR == 1)

   CW_Rend

end


%=========================================================================
%
%  Accomplish Linear Quadratic Regulator Rendezvous
%
%  1.  Starting values: position and velocity of the target, ref, and micro at CW rend time
%  2.  Calculate the A matrix, set up the B, Q, and R matrices
%  3.  Solve for the gain matrix, K
%  4.  Iterate
%      A.  Calculate the necessary control input
%      B.  Propagate one step
%      C.  Repeat until successful rendezvous is achieved
%
%=========================================================================

if LR == 1

   LQR_Rend

elseif CWLR == 1

   r_micro_ijk_tmp = r_micro_ijk(rend_time,:);

   v_micro_ijk_tmp = v_micro_ijk(rend_time,:);
```

```
    r_tgt_act_tmp = r_tgt_act_ijk(rend_time,:);

    v_tgt_act_tmp = v_tgt_act_ijk(rend_time,:);

    r_ref_ijk_tmp = r_ref_ijk(rend_time,:);

    v_ref_ijk_tmp = v_ref_ijk(rend_time,:);

    LQR_Rend

end


%=========================================================================
%
%  Print Output Values
%
%=========================================================================


delta_r = delr
ro_delta_theta = dist
delta_z = delz

if CW == 1

    pert
    dragtgt
    dragmic
    rend_time
    timestep
    delta_v_cw1
    delta_v_cw2
    delta_v_accum
    dist_at_rend_time = r_mag_rel_cw

elseif CWLR == 1

    pert
    dragtgt
    dragmic
    rend_time
    pt
    rend_time+pt
    timestep
```

```
    Q_mag
    R_mag
    delta_v_cw1
    delta_v_lqr
    delta_v_accum
    dist_at_rend_time = r_mag_rel_cw
    final_vel = vel_now
    final_dist = dist_now

elseif LR == 1

    pert
    dragtgt
    dragmic
    pt
    timestep
    Q_mag
    R_mag
    delta_v_lqr
    delta_v_accum
    final_vel = vel_now
    final_dist = dist_now

end


%=============================================================
%
%  Draw Desired Plots
%
%=============================================================

Do_Plots


%=============================================================
%
%  End of Program
%
%=============================================================

run_time = toc
```

Bibliography

1. Chobotov, Vladimir A. (ed). *Orbital Mechanics* (2nd Edition). Washington DC: American Institute of Aeronautics and Astronautics, Inc., 1996.

2. Irvin, David J., Jr., *A Study of Linear Vs. Nonlinear Control Techniques for the Reconfiguration of Satellite Formations*. MS Thesis, AFIT/GA/ENY/01M-02, Graduate School of Engineering, Air Force Institute of Technology (AETC), Wright-Patterson AFB OH, March 2001.

3. Kreyszig, Erwin. *Advanced Engineering Mathematics* (8th Edition). New York NY: John Wiley & Sons, Inc., 1999.

4. McLaughlin, Craig A., and others. "Modeling Relative Position, Relative Velocity, and Range Rate for Formation Flying." AAS 01-457, 2001.

5. National Air and Space Agency. "Defense Meteorological Satellite Program (DMSP) Satellite F13 Source/Platform." http://ghrc.msfc.nasa.gov:5721/source_documents/dmsp_f13.html. 20 February 2003.

6. Ogata, Katsuhiko. Modern Control Engineering (4th Edition). Upper Saddle River NJ: Prentice Hall, Inc., 2002.

7. "PLA Said Developing Anti-Satellite Weapons to Counter US NMD, TMD Systems." *Ming Pao*, Hong Kong January 2001.

8. Swank, Aaron J. and others. "Long-Duration Analysis of the J_2-Model Equations of Relative Motion for Satellite Clusters." AAS 02-185, 2002.

9. Tragesser, Steven G. *Class Notes* (MECH 532, MECH 533). Wright-Patterson AFB OH, Graduate School of Engineering, Air Force Institute of Technology (AETC), 2002.

10. Vallado, David A. *Fundamentals of Astrodynamics and Applications*. New York: McGraw-Hill, 1997.

11. Wie, Bong. *Space Vehicle Dynamics and Control*. Washington DC: American Intstitute of Aeronautics and Astronautics, Inc., 1998.

12. Wiesel, William E. *Spaceflight Dynamics* (2nd Edition). Boston MA: Irwin McGraw-Hill, 1997.

13. Wertz, James R. *Spacecraft Attitude Determination and Control*. Dordrecht, Holland: D. Reidel Publishing Company, 1978.

14. Yi, Tung. "China Competes Ground Tests of Anti-Satellite Weapon." *Sing Tao Jih Pao*, Hong Kong January 2001.

REPORT DOCUMENTATION PAGE

Form Approved
OMB No. 074-0188

1. REPORT DATE *(DD-MM-YYYY)*	2. REPORT TYPE	3. DATES COVERED *(From – To)*
14-03-2003	**Master's Thesis**	Jul 2002 – Mar 2003

4. TITLE AND SUBTITLE

A STUDY OF CONTROL LAWS FOR MICROSATELLITE RENDEZVOUS WITH A NONCOOPERATIVE TARGET

5a. CONTRACT NUMBER

5b. GRANT NUMBER

5c. PROGRAM ELEMENT NUMBER

6. AUTHOR(S)

Tschirhart, Troy, A., Major, USAF

5d. PROJECT NUMBER

5e. TASK NUMBER

5f. WORK UNIT NUMBER

7. PERFORMING ORGANIZATION NAMES(S) AND ADDRESS(S)
Air Force Institute of Technology
Graduate School of Engineering and Management (AFIT/EN)
2950 P Street, Building 640
WPAFB OH 45433-7765

8. PERFORMING ORGANIZATION REPORT NUMBER

AFIT/GAI/ENY/03-3

9. SPONSORING/MONITORING AGENCY NAME(S) AND ADDRESS(ES)

10. SPONSOR/MONITOR'S ACRONYM(S)

11. SPONSOR/MONITOR'S REPORT NUMBER(S)

12. DISTRIBUTION/AVAILABILITY STATEMENT

APPROVED FOR PUBLIC RELEASE; DISTRIBUTION UNLIMITED.

13. SUPPLEMENTARY NOTES

14. ABSTRACT

The feasibility of using a microsatellite to accomplish an orbital rendezvous with a noncooperative target is being evaluated. This study focused on the control laws necessary for achieving such a rendezvous. The relative motions of the microsatellite and the target satellite were described using Hill's equations and two different controller methodologies were investigated. An impulsive thrust controller based on the Clohessey-Wiltshire solution was found to use little fuel, but was not very robust. A continuous thrust controller using a Linear Quadratic Regulator was found to be more robust, but used much more fuel. As a final solution, a hybrid controller was evaluated which uses the low thrust Clohessey-Wiltshire approach to cover most of the necessary distance, and then switches to the Linear Quadratic Regulator method for the final rendezvous solution. Results show that this approach achieves rendezvous with a reasonable amount of control input.

15. SUBJECT TERMS

Microsatellite, Rendezvous, Control, Dynamics

16. SECURITY CLASSIFICATION OF:			17. LIMITATION OF ABSTRACT	18. NUMBER OF PAGES	19a. NAME OF RESPONSIBLE PERSON
a. REPORT	b. ABSTRACT	c. THIS PAGE			Dr Steven G. Tragesser, AFIT/ENY
U	U	U	UU	91	19b. TELEPHONE NUMBER *(Include area code)* (937) 255-6565, ext 4286; e-mail: steven.tragesser@afit.edu